Fabrication and characterisation of RGB LEDs based on nanowire technology

Patrik Olausson, patrikolausson95@gmail.com
Faculty of Engineering
Division of Solid State Physics
Lund University

Principal Supervisor: Professor Lars Samuelson, lars.samuelson@ftf.lth.se
Assistant Supervisor: Ph.D. Olof Hultin, RISE, olof.hultin@ri.se
Examiner: Associate Professor Carina Fasth, carina.fasth@ftf.lth.se

May 31, 2019

LUND UNIVERSITY

RI.SE

Abstract

The white light LEDs of today are usually based on a blue LED and a phosphor, converting the blue light to longer wavelengths. While these phosphor-converted LEDs are extremely efficient compared to incandescent light or fluorescent light, there is still plenty of room for improvement. In the conversion between blue light and light of lower energy approximately 25-45 % of the radiant power is lost as heat [1]. A more efficient solution is to use white light sources based on RGB LEDs. Since these LEDs do not require phosphor conversion the efficiency has potential to be much higher compared to today's white light sources.

High efficiency blue LEDs are based on an InGaN quantum well and barrier layers of GaN. By altering the In content in InGaN the bandgap can be tuned for emission from UV to red light, which makes the material system a good candidate to be used in fabrication of RGB LEDs. In green and red LEDs the In content in the quantum well is higher compared to blue LEDs which gives rise to more strain between the quantum well and GaN barrier layers. The strain induces piezoelectric charges which spatially separates electrons and holes in the quantum well leading to lower radiative recombination efficiency (quantum-confined Stark effect). The use of InGaN barrier layers would thus enable fabrication of red and green LEDs of higher efficiency, but the main problem is that it is very hard to synthesise thick layers of InGaN with high material quality. The poor crystal quality is partly due to strain induced dislocations and partly due to phase separation and In content fluctuations [2], which will reduce the efficiency of the device [3].

However it has been shown that thick InGaN layers of high material quality can be synthesised in MOCVD grown nanocrystals of InGaN. These nanocrystals, or platelets (truncated pyramids with a flat c-plane), can be used as dislocation free substrates for growth of LEDs, which enables the use of InGaN barrier layers instead of GaN. The strain between the quantum well and barriers in In rich quantum wells is thus reduced which makes it possible to fabricate red and green LEDs of high efficiency. The reduced strain between the barriers and the quantum well leads to a decrease of the quantum-confined Stark effect and therefore potential of higher efficiency LEDs.

In this thesis the potential of nano RGB LEDs based on InGaN and GaN platelets is evaluated and the results are promising. During the project an LED device design for LEDs based on (In)GaN platelets was developed, characterised (electrically and electroluminescence) and optimised (spacer layer thicknesses, contact materials). The implemented device design works well. Parasitic currents outside the active area are negligible and the devices show much improved stability compared to previous designs.

The device design is based on parallel connected platelets in the device area and lifted bond pads outside of the device area. The bond pads are lifted by a thick spacer layer (resist) in order to enable easy bonding and avoid shunt current. A range of devices of different size were studied, from single platelets (<1µm) to tens of thousands of platelets (400µmx400µm) and the crystal homogeneity is shown to be very important for the device performance. The current rectification is excellent for single platelet devices but decreases with increased number of platelets in the device.

While work lies ahead in improving homogeneity, efficiency and device design, this technology is unique in achieving high quality material with very high In content and an extremely small light emission area. Not only are these structures interesting for high-efficiency RGB illumination, but also for microLED displays - potentially with pixel size an order of magnitude smaller than what is possible today.

Populärvetenskaplig sammanfattning

Ultra-effektiv belysning baserad på nanotrådsteknik

Den ökade växthuseffekten som följd av användandet av fossila bränslen kombinerat med jordens stadigt ökande befolkning, gör att användandet av jordens resurser måste effektiviseras. En stor del av dagens energiförbrukning går åt till belysning, vilket gör effektiviseringen av dagens ljuskällor till en mycket viktig fråga. Majoriteten av dagens vita belysning baseras på att lägga en spänning över ett halvledarmaterial (InGaN), vilket leder till att blått ljus sänds ut (emitteras). Det blåa ljuset absorberas av ett lysämne (fosfor) som sedan återemitterar ljus av längre våglängder. Kombinationen av det blåa ljuset och ljuset av längre våglängder uppfattas som vitt ljus, men i omvandlingen från blått ljus till ljus av längre våglängder går 25-45 % av strålningseffekten förlorad i form av värme [1]. Denna process för att skapa vitt ljus är därför ineffektiv och ett effektivare sätt att skapa vitt ljus är att använda sig av separata röda, gröna och blåa dioder. Denna typ av ljuskälla kallas för RGB lysdiod (LED).

Ett sätt att tillverka dioder som emitterar olika färger är att använda halvledaren InGaN (indium-gallium-nitrid) och variera andelen indium (In). Ju mer indium legeringen innehåller, desto längre blir våglängden, vilket därför kan justeras för att ge emission av rött, grönt och blått ljus. Högeffektiva blåa dioder baseras på ett aktivt område bestående av ett tunt lager InGaN, omslutet av tjocka GaN (gallium-nitrid) barriärer. Avståndet mellan atomerna i det aktiva området (InGaN) skiljer sig från avståndet mellan atomerna i barriärerna (GaN), och ju mer indium det aktiva området innehåller desto större blir skillnaden. På grund av skillnaden i avstånd mellan atomerna uppstår mekaniska spänningar mellan det aktiva området och barriärerna, vilket leder till minskad effektivitet hos dioderna. I blåa dioder innehåller det aktiva området en låg andel indium och spänningen är därför liten mellan det aktiva området och barriärerna, men för gröna och röda dioder ökar spänningen på grund av ökad andel In i det aktiva området. Effektiviteten är därför lägre för gröna och röda dioder jämför med blåa.

För att minska spänningen mellan det aktiva området och barriärerna i gröna och röda dioder skulle man kunna använda InGaN som barriärmaterial istället för GaN. Indium innehållet i barriärerna är lägre än indium innehållet i det aktiva området, så det kommer fortfarande vara spänning mellan barriärerna och det aktiva området, men mindre spänning jämfört med om GaN barriärer används. Problemet med att använda InGaN barriärer är att det är väldigt svårt att framställa tjocka lager av InGaN med hög material kvalité, vilket leder till lägre effektivitet hos dioden. Lösningen på problemet är att använda nanoteknik. Genom att framställa extremt små (i storleksordningen miljarddelsmeter) kristaller av InGaN med formen av trunkerade pyramider (platelets) och sedan använda dessa kristaller som substrat, möjliggörs framställandet av tjocka lager av InGaN med hög material kvalité. Denna metod har därför potential att användas för tillverkning gröna och röda dioder av hög effektivitet, vilket kan användas i tillverkning av hög effektiva RGB LEDs.

Att tillverka komponenter av nanokristaller medför en rad utmaningar som skiljer sig från traditionell LED-tillverkning. Till exempel ställer det extremt höga krav på homogenitet och kontroll av lagertjocklek över stora ytor.

I detta projekt har LED designen för LEDs baserade på dessa nanokristaller (platelets) utvecklats och karakteriserats genom att använda avancerade tillverkningsmetoder på nanoskalan (tillexempel: atomlagerdeposition, spin-coating, sputtring, rapid thermal processing, UV-litografi, elektronstråle-litografi och olika typer av etsning). I Figur 1 visas en sketch av LED designen och Figur 2 visar ett färdigt prov.

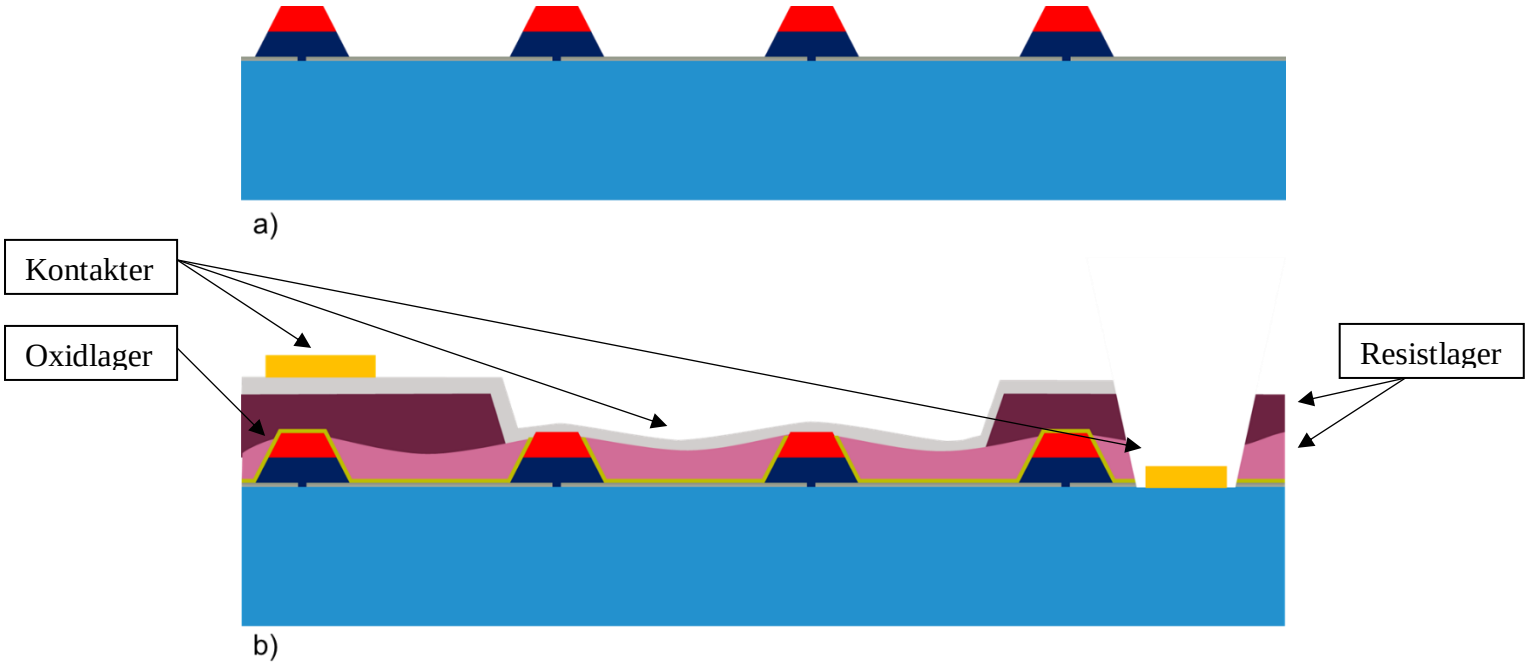

Figur 1
Schematiska skisser över LED designen.

- *a) Skissen visar fyra nanokristaller. Den röda delen motsvarar den ena InGaN barriären och den blåa delen motsvarar den andra barriären. Mellan barriärerna finns det aktiva området, som är väldigt tunt. Det är från detta område ljuset sänds ut (emitteras).*
- *b) Skissen visar ett färdigt prov. Ett tunt isolerande oxidlager (gult lager i bilden) har deponerats på provet och etsats bort från topparna av de två nanokristallerna i mitten (komponentarean) och även i området där den högra kontakten är placerad. Det första resistlagret (rosa lager i bilden) möjliggör oxidetsning från enbart topparna av nanokristallerna och det andra resistlagret (lila lager i bilden) lyfter upp kontakterna utanför komponentarean för att undvika läckström till kristaller utanför komponentarean. Den gråa kontakten är transparent och består av ITO (indium-tenn-oxid) och de gula kontakterna består av titan och guld. Genom att lägga olika elektriska potentialer på de gula kontakterna uppstår en spänning mellan barriärerna (rött och blått lager i bilden) vilket inducerar ljusemission från det aktiva området.*

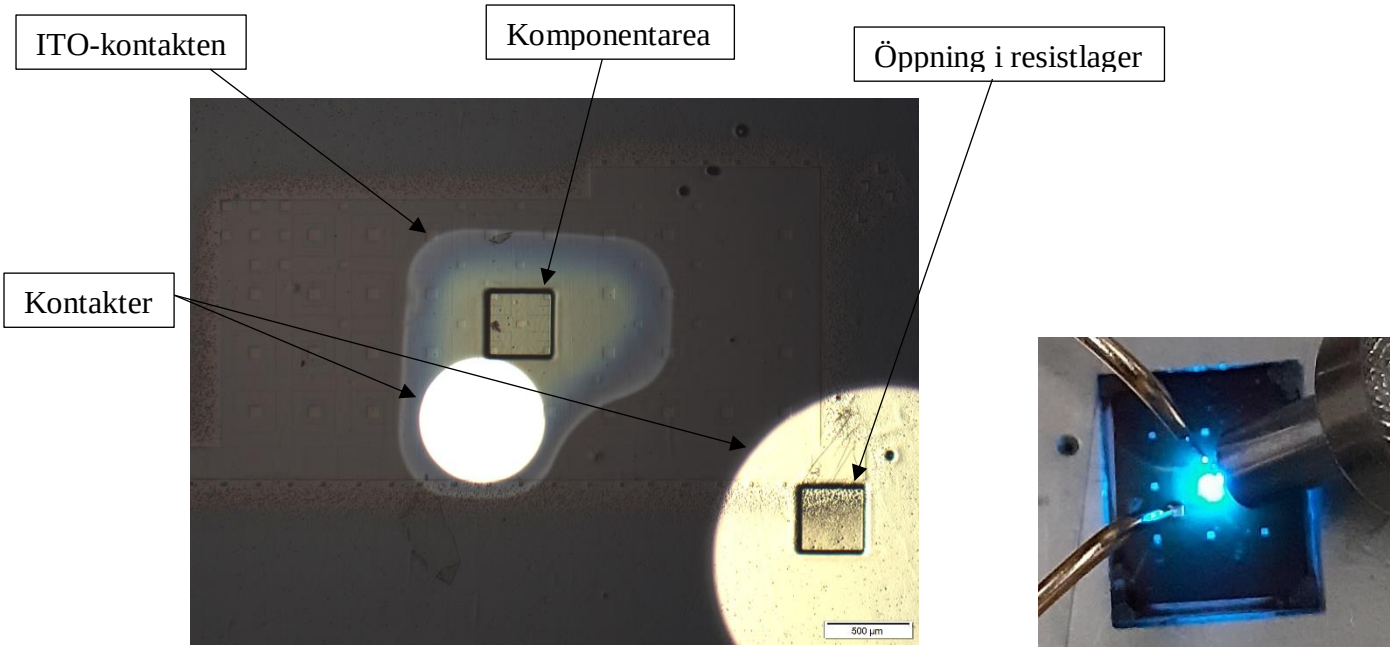

Figur 2
Bilder som visar ett färdigt prov.

- *A) Provets olika delar är indikerade med pilar (jämför med Figur 1 B).*
- *B) Bild av provet när en konstant spänning är pålagd och emissionsspektrumet mäts. Till vänster i bilden syns två probar och till höger syns en optiskfiber som är ansluten till en spektrometer.*

Från de elektro-optiska mätningarna uppskattades effektiviteten av dioderna genom att jämföra strålningseffekten från ett prov med strålningseffekten från en diod av känd effektivitet. Effektiviteten visade sig vara väldigt låg och en möjlig anledning till den låga effektiviteten är att det i komponentarean finns kristaller som är betydligt högre än nanokristallerna och dessa kristaller blir därför kortslutna (båda barriärerna blir kontakterade till toppkontakten). Det blir alltså ingen spänning över det aktiva området hos dessa kristaller, vilket drar ner effektiviteten hos dioden.

Komponenter bestående av enskilda nanokristaller visar utmärkt likriktning (dioden leder bara ström i ena riktningen, vilket är karaktäristiskt för dioder), men likriktningen minskar med ökad storlek av komponentarean. Sannolikheten för att nanokristaller blir kortslutna ökar när antalet nanokristaller i komponentarean ökar vilket förmodligen är orsaken till den minskade likriktningen med ökad komponentarea.

Tekniken behöver utvecklas ytterligare men har potential att användas i tillverkning av RGB LEDs eftersom den kan möjliggöra tillverkandet av högeffektiva röda och gröna nitrid-LEDs. Tekniken är unik i att möjliggöra hög materialkvalité med väldigt hög indiumkoncentration, och en extremt liten ljusemissionsarea. Den lilla ljusemissionsarean gör strukturerna intressanta för andra applikationer utöver RGB LEDs, tillexempel som mikrometerstora LEDs i högupplösta displayer.

Preface/Acknowledgements

This Master's thesis project was conducted October 2018-June 2019. The main goal was to explore the potential of RGB LEDs based on InGaN nanocrystals and develop a device design for LEDs based on these crystals.

The project was partly funded by the Swedish Energy Agency, EELYS "Ultra efficient RGB-lighting based on nanowire technology", RISE Research Institutes of Sweden, NanoLund and Lund University

I want to thank the following people which made this project possible:

My supervisors, Lars Samuelson and Olof Hultin, thank you for great discussions and supervision. A special thanks to Olof, who also has been my lab coach and taught me how to use all tools needed for the project, and thank you for always taking the time to help me.

The Nitride group, for interesting meetings and discussions. A special thanks to Taiping Lu and Zhaoxia Bi for excellent epitaxy work. I also want to thank Ali Nowzari for your great ideas and advices regarding the device design.

The lab staff, for help with tools and equipment at Lund Nano Lab.

Last, I want to thank my family for all your support.

Table of contents

1 Introduction

One of the greatest challenges mankind is facing right now is the reduction of greenhouse gas emission, which requires a switch from fossil based fuels to renewable fuel sources. The energy consumption needs to be reduced and the only possibility is to use the energy more efficiently.

This Master's thesis project is a part of a collaboration between Lund University and RISE Research Institutes of Sweden and will focus on the development of high efficiency RGB LEDs, which is one step on the way towards reduced energy consumption.

Today most white LEDs are based on high efficient blue InGaN diodes. The blue light is then converted by phosphors to light of longer wavelengths and the combination of the blue light and the light of longer wavelengths gives rise to white light. In the conversion approximately 25-45 % of the radiant power is lost as heat [1]. A more efficient solution is to fabricate LEDs where the white light is based on the combination of red, green and blue diodes. This type of white LEDs is called RGB LEDs because they consist of separate red, green and blue diodes. RGB LEDs have potential as a white light source of high efficiency, but this is not the only advantage of these LEDs. Because of the separate red, green and blue diodes, RGB LEDs enable to control the relative intensities of the red, green and blue diodes, which can be used in order to increase the quality of the light by tuning the colour temperature.

The bandgap of InGaN will decrease with increased In content [4][5], which makes it possible to tune the bandgap for emission from UV to red light, see Figure 1.1 A. In green and red LEDs the In content in the quantum well is higher compared to blue LEDs which gives rise to more strain between the quantum well and GaN barrier layers compared to the strain in blue LEDs. The strain induces piezoelectric charges which spatially separates electrons and holes in the quantum well leading to lower radiative recombination efficiency (quantum-confined Stark effect) [6]. The use of InGaN barrier layers would thus enable fabrication of red and green LEDs of higher efficiency, but the main problem is that it is very hard to synthesise thick layers of InGaN with high material quality. The poor crystal quality is partly due to phase separation and In content fluctuations, but also due to strain induced dislocations [2], which will reduce the efficiency of the device [3].

The external quantum efficiency is very high in nitride LEDs emitting in the blue region but low for emission of green and red [6], see Figure 1.1 B.

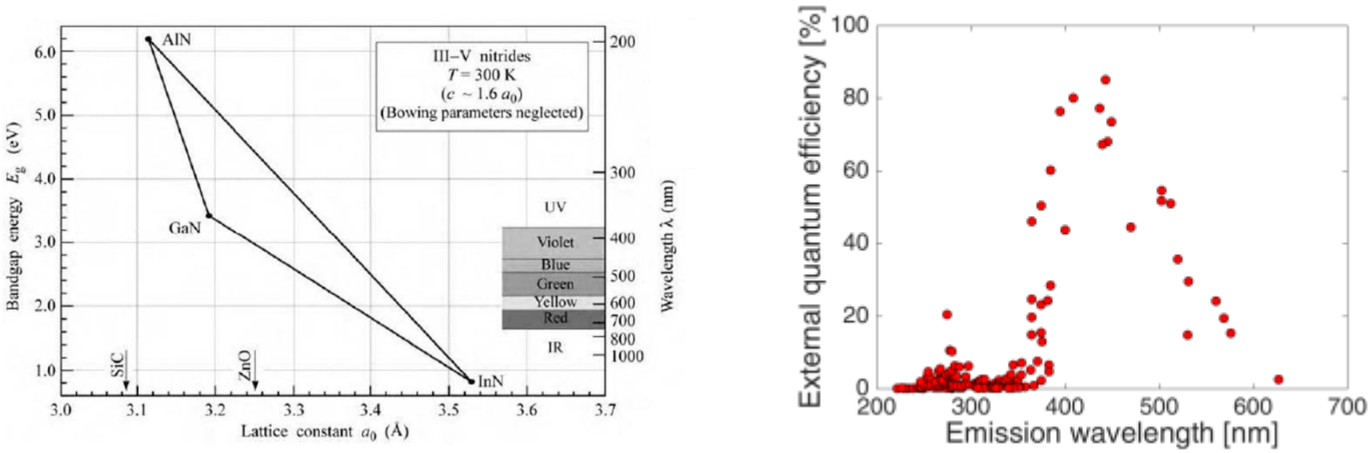

A B

Figure 1.1

A) Graph showing bandgap energy versus lattice constant for III-IV nitride semiconductors. The bandgap of InGaN spans over the entire visible spectrum. Image adapted from [5]

B) Graph showing external quantum efficiency versus emission wavelength for nitride LEDs. The efficiency is very high in the blue region. Image adapted from [6]

Research at Lund University has led to the development of a method to grow dislocation free, stable InGaN nanocrystals with high In content [7]. These crystals or platelets (truncated pyramids with a flat c-plane) can be used as dislocation free substrates for growth of LEDs, and enables use of InGaN barriers instead of GaN barriers, which will reduce the lattice mismatch between the barriers and the quantum well in green and red diodes [8]. These platelets thus have potential to be used in fabrication of high efficiency red and green diodes.

Another potential application for these platelets in addition to be used in fabrication of high efficiency RGB LEDs, would be as micro-sized LEDs in microLED displays. When the LED structure becomes smaller the ratio between area and volume will increase and the impact of non-radiative surface recombination will thus be more significant. Today's red LEDs are usually based on AlInGaP, which has higher surface recombination than nitride LEDs. Micro-sized red nitride LEDs has therefore potential to be used in high efficiency microLED displays [8].

It has been shown that it is possible to fabricate RGB LEDs based on the InGaN platelets which Lund University is growing [8], however the previous design is not suitable for permanent connections by bonding and is limited by a semi-transparent top contact. The goal of this project is to develop and evaluate a new nanoplatelet LED device design suitable for permanent bonding and packaging. The device design should enable efficient electrical injection to the nanocrystals, high shunt resistance, efficient light extraction, as well as be

reproducible and robust. Permanent bonding is necessary in order to be able to fabricate a packaged LED demonstrator and also enables more advanced characterisation.

In next chapter theory about LEDs in general and LEDs based on quantum wells and nanowires in particular is presented. Then the growth process of InGaN platelets is briefly described and the chapter ends with a description of the previous nanoplatelet LED device design. The development process is described in chapter 3, then in chapter 4 the results are presented together with discussion of the results and finally the report ends with an overall conclusion and outlook (chapter 5).

2 Theory

An LED basically consists of a p-n junction. On the p-doped side impurities with fewer valence electrons than the host atoms have been incorporated into the crystal structure giving rise to electron vacancies. Another way is to think of the missing electrons as quasiparticles with equal charge as electrons but with opposite sign. These quasiparticles are called holes and because of their positive charge they will move in the opposite direction in an electric field compared to electrons. On the n-side impurities with an extra electron in their outermost shell have been incorporated into the crystal structure. The holes on the p-side and the extra electrons on the n-side are only loosely bond to their impurity atoms and are easily ionised, which gives rise to mobile charge carriers and electric conductivity. Because of the small energy needed in order to ionise the impurity atoms, the impurity atoms will correspond to states close to the valence band and conduction band in the crystal respectively, see Figure 2.1.

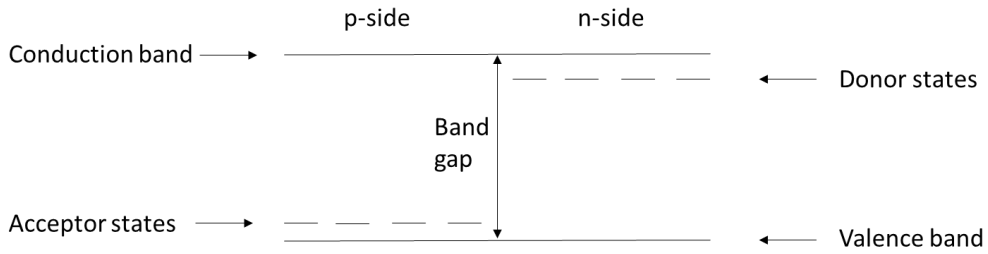

Figure 2.1
Schematic diagram of the band structure of a p-n junction.

Since the impurity atoms are easily ionised the concentration of holes on the p-side is higher than on the n-side, and vice versa for the electron concentrations. If an electron and a hole meet they will recombine and the region between the p- and n-side will therefore be depleted of charge carriers, this region is called the depletion region. In the depletion region the immobile ionised impurity atoms will give rise to an electric field. On the p-side the impurity atoms have created holes by accepting electrons from the valence band and on the n-side the impurity atoms have donated electrons to the conduction band, therefore there are negative ions on the p-side and positive ions on the n-side. The electric field is thus directed from the n-side to the p-side, and will bend the bands according to Figure 2.2.

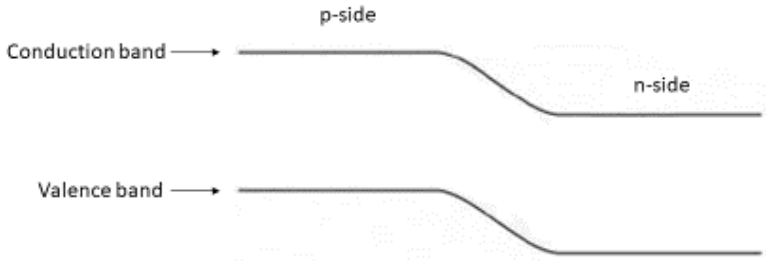

Figure 2.2
Schematic diagram of the band structure of a p-n junction in thermodynamic equilibrium.

If a bias is applied in the forward direction (negative bias on n-side) the band on the n-side will raise compared to the p-side and the potential barrier between the n- and p-side will decrease. Because of the lower barrier electrons will be injected to the p-side and holes will be injected to the n-side, and recombination can occur. The number of injected charge carriers and thus the current (I) depends exponentially on the applied voltage, see eq. (2.1), where e is the elementary charge, V is the applied voltage, k is Boltzmann's constant and T is the temperature. If a bias is applied in the reverse direction electrons will drift from the p-side to the n-side and the holes will drift in the opposite direction, this gives rise to a small saturation current, I_s, in the reverse direction.

$$I = I_s\left(e^{eV/kT} - 1\right) \qquad (2.1)$$

Equation (2.1) is called the ideal diode equation and real diodes will deviate from this equation. The IV characteristic of real diodes is better described by eq. (2.2), where n_{ideal} is the ideality factor of the diode, R_p is a shunt resistance parallel to the ideal diode and R_s is a resistance in series with the ideal diode.

$$I - \frac{V - IR_s}{R_p} = I_s e^{e(V-IR_s)/(n_{ideal}kT)} \qquad (2.2)$$

The series resistance could be due to contact resistance or resistance of the neutral regions and the parallel resistance could be due to the resistance in a channel that bypasses the p-n junction [5]. In Figure 2.3 the effect of parallel and series resistance on the IV characteristics is shown and compared with the characteristics of an ideal diode.

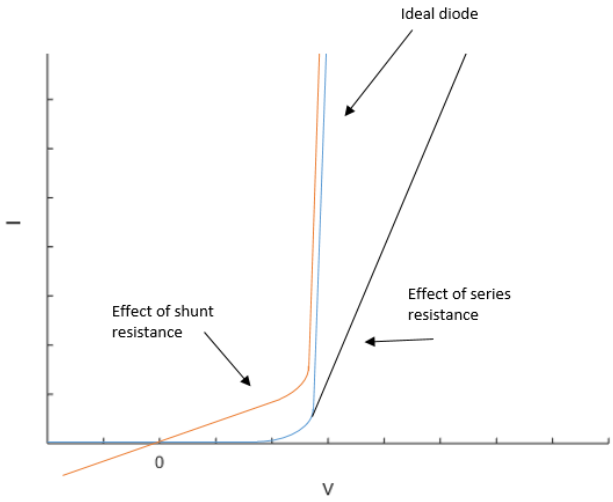

Figure 2.3
Effect of shunt and series resistance on the IV-characteristics of a diode.

As we can see from Figure 2.3 series resistance will give rise to a smaller slope at high forward current compared to the ideal diode and the parallel resistance (shunt) will give rise to a slope below the threshold voltage.

The recombination process in an LED can either be non-radiative or radiative. In principle three different types of recombination processes can occur [5]. A charge carrier can fall into a trap energy level in the bandgap and then in another step completing the recombination by falling down to the lower band. This process is called Shockley-Read-Hall recombination and is a non-radiative recombination process, the energy is released as heat (vibrations of crystal structure). A second recombination process is that an electron from the conduction band falls down into a hole in the valence band and the energy difference is released by emitting a photon, this process is a radiative recombination process. Since the radiative recombination process requires that an electron and hole meet, the probability of radiative recombination is proportional to the product of the electron and hole concentrations [6]. The third recombination process is Auger recombination. In Auger recombination the released energy in the transition of an electron from the conduction band to the valence band is released by emitting another electron or hole.

In diodes radiative recombination is of course the preferred event and a figure of merit is the so called quantum efficiency. The internal quantum efficiency is defined as the probability of radiative recombination divided by the total probability of recombination [9], see eq.(2.3), where r_r and r_{nr} is the radiative recombination coefficient and non-radiative recombination coefficient respectively.

$$\eta_{int} = \frac{r_r}{r_r + r_{nr}} \qquad (2.3)$$

However, all photons created in the LED will not contribute to the light emitted from the device, due to reflections at the surface. This effect is particularly high for semiconductors, which usually have high refractive indexes and therefore a lot of rays will undergo total internal reflection [9]. An important factor for LED devices is therefore the extraction efficiency, which is the efficiency by which internal photons can be extracted from the LED structure. The product of the internal quantum efficiency and the extraction efficiency is called the external quantum efficiency (EQE). Another way to determine the efficiency of an LED is to calculate the wall-plug efficiency (WPE), which is defined as the ratio of the total light output power (LOP) divided by the total electrical input power.

2.1 Quantum well LEDs

In LEDs based on p-n homojunctions the charge carriers will recombine in a region determined by the diffusion length of the carriers. One way to decrease the size of this region and thus also increase the carrier concentrations is to fabricate LEDs based on heterostructures. By synthesising a heterojunction consisting of a thin layer of a smaller bandgap material sandwiched between larger bandgap materials (barriers) the charge carriers will be confined in a region determined by the thickness of the smaller bandgap material. This type of heterojunction structure is called a quantum well and if the width of the quantum well is much smaller than the diffusion length of the charge carriers a more efficient recombination process will occur [5]. As described in chapter 2, the probability of radiative recombination is proportional to the product of electron and hole concentrations, which will be much higher in quantum wells compared to homostructures and the radiative recombination process is thus more efficient in LEDs based on quantum wells. In order to reduce the leakage of charge carriers from the quantum well to the barriers a blocking layer of a high bandgap material is often inserted at the interface between the quantum well and the barriers [5]. Usually a blocking layer is only needed on the p-side to block electrons and not on the n-side to block holes because the probability of a hole escaping from the quantum well is much lower than for an electron due to the lower mobility of holes compared to electrons [5].

A challenge associated with the use of heterostructures is that strain will arise due to difference in lattice constants between the barriers and the quantum well. This could give rise to poor material quality and non-radiative recombination centres (misfit dislocations and point defects). For planar LEDs the strain in the layers of the device is partly induced due to lattice mismatch between the layers of the LED and the foreign substrate, which gives rise to a large concentration of threading dislocations through the device, and partly induced by lattice mismatch between the barriers and the quantum well. For homogeneous nanowires, inherited strain and dislocations from the substrate will disappear after a distance on the order of the wire diameter [10]. Thus for LEDs based on nanowires all strain is induced by lattice mismatch between the active layers, and if the thickness of the layers is below the critical thickness for formation of dislocations the LED will be defect free, but not free from strain [10].

For heterostructures based on GaN the strain is especially deleterious because the strain gives rise to piezoelectric charges which will spatially separate electrons and holes in the quantum well [6], see Figure 2.4.

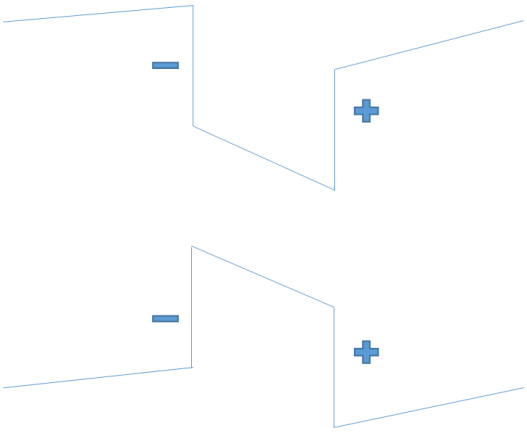

Figure 2.4
Schematic diagram showing the band structure of a quantum well under influence of the quantum-confined Stark effect.

The effect shown in Figure 2.4 is called quantum-confined Stark effect and will drastically reduce the radiative recombination efficiency. The electrons will prefer to be in the right side of the quantum well and the holes prefer the left side, this spatial division of electrons and holes is the reason for the reduced radiative recombination efficiency [11].

As mentioned in the introduction (chapter 1) the bandgap of InGaN will decrease with increased In content, this means that for green and red LEDs the quantum well will have a higher In content and therefore the strain due to lattice mismatch between the well and the GaN barriers will be higher in comparison to blue LEDs and the quantum-confined Stark effect will thus be more significant. However, the quantum-confined Stark effect can be reduced by using dislocation free InGaN platelets developed at Lund University as substrates for growth of LEDs, which enables use of InGaN barriers instead of GaN barriers, see Figure 2.5. The lattice mismatch between the barriers and the quantum well in green and red diodes is thus reduced as well as the quantum-confined Stark effect. This is the central point on which this project's approach to achieve high efficiency red and green nitride LEDs is based.

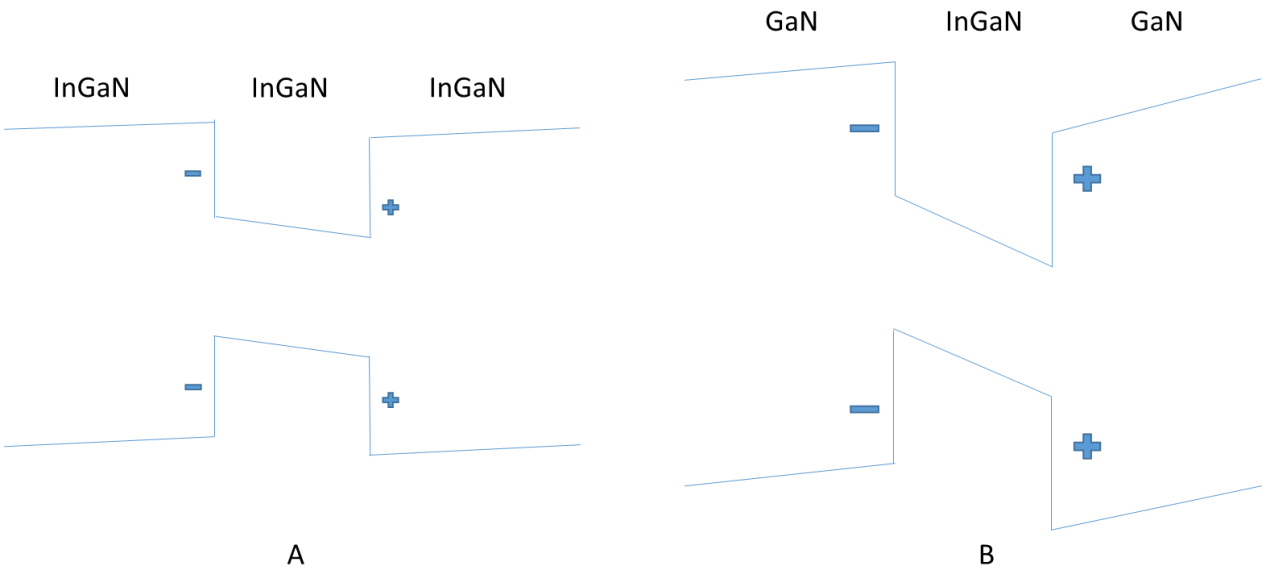

Figure 2.5
Sketches of quantum wells under influence of piezoelectric charges. If InGaN barriers are used (A) instead of GaN (B) the strain between the quantum well and the barriers is reduced, which leads to lower influence of the quantum-confined Stark effect and thus potential of higher radiative recombination efficiency. Note that there still will be strain between the quantum well and barriers even in the case of InGaN barriers due to the higher In content in the quantum well compared to the barriers. The band gap of the barriers will also be smaller compared to the GaN barriers.

2.2 Nanowire LEDs

One of the greatest advantages of LEDs based on nanowires compared to planar LEDs is the possibility to grow dislocation free nanostructures on top of foreign substrates. The small footprint of the nanowires filters out most of the dislocations from the substrate and dislocations that nevertheless extends from the substrate to the nanowire will be terminated at the wire side facets within a distance corresponding to the diameter of the nanowire [10]. This enables growth of material combinations that would not be possible with planar structures without creating a lot of dislocations.

A problem related to nitride LEDs is the so called droop, which is a reduction of the efficiency at high current densities [10]. The reason is still not clarified but it has been shown that planar LEDs grown on GaN substrates (very expensive and rarely used for LEDs) show considerably less droop compared to LEDs grown on foreign substrates, which indicates that the origin of droop at least partly is related to the dislocation density and thus could be reduced by the use of nanowire LEDs instead of planar LEDs [12].

The common way to decrease the dislocation density in planar LEDs is to grow a thin GaN buffer layer on top of the substrate which is then overgrown with a thicker layer. Most of the dislocations will be restricted to the thin layer, which gives a lower dislocation density in the active layers ($< 10^9$ cm^{-2}) [10], but still higher than the dislocation density in nanowire based LEDs.

A second advantage of nanowire LEDs is that new growth facets are available, for instance the non-polar m-plane in GaN [13]. Nanowire LEDs based on m-plane quantum wells are not influenced by quantum-confined Stark effect, and thus interesting for high efficiency nitride LEDs.

A third advantage of nanowire LEDs is that they enable integration of LEDs of different colours on the same substrate [14], which could be an important property in development of RGB LEDs.

A fourth reason to use nanowire LEDs is the potential to fabricate microLEDs with submicron pixel size. Today's planar microLEDs typically have a pixel pitch of 10 µm [15], an order of magnitude larger than the pixel pitch we use in this project. In order to present virtual reality a resolution of 9600 x 9000 pixels is needed, and the pixel density needs to be more than 2000 pixels per inch (ppi) [16]. Today's LCD 4k resolution only has a pixel density of 1058 ppi, but the use of nanowires enables submicron pixel sizes, giving a pixel density well beyond 5000 ppi [16].

The fifth and last advantage mentioned in this chapter is the ability of nanostructures to increase the light extraction efficiency [17].

Despite the great number of advantages of nanowire LEDs compared to planar LEDs, there are a lot of challenges to overcome before nanowire LEDs can replace the planar structures on the market. The greatest challenges are related to the high uniformity and precision required in growth and processing of structures on the nanoscale, but also surface properties, such as

surface recombination and surface defects, are very important due to the high surface to volume ratio of nanostructures. It has been shown that surface passivation can reduce the number of surface states and thus non-radiative recombination in nanowire LEDs [18][19].

2.3 Growth of (In)GaN platelets

It is very challenging to fabricate high efficiency planar LEDs for emission of red and green using InGaN as active layer. The high In content of the active layer in red and green diodes leads to strong impact of the quantum-confined Stark effect and InGaN barrier layers are thus needed in order to reduce this effect and increase the efficiency of the device. But it is hard to grow thick planar layers of InGaN of high material quality partly due to phase separation and In content fluctuations [2], but also due to lattice mismatch between the substrate and the InGaN layer and lattice mismatch between GaN and InN [7].

By using InGaN platelets as dislocation free substrates for growth of LEDs, thick dislocation free layers of InGaN can be synthesised and used as barrier layers, which reduces the quantum-confined Stark effect in red and green diodes. Platelets are III-N nanocrystals with the shape of truncated pyramids with a flat c-plane, which can be used as dislocation free substrates.

(In)GaN platelets can be grown on top of an n-doped GaN film by metal-organic vapour phase epitaxy (MOVPE). The platelets will grow in areas defined by openings in a growth mask of Si_3N_4. The crystals grown are pyramid shaped and the growth rate as well as the growth uniformity is improved by using GaN nanowires as seeds for the growth [7]. The grown pyramid shaped crystals can be reshaped by cutting of the Ga flow at a temperature above the sublimation temperature of GaN, then Ga atoms will dissociate from the crystal which gives rise to a surface-bound layer of Ga. In order to minimise the surface energy a flat top surface is formed, which is perpendicular to the [0001] direction in the crystal. This flat surface is called the c-plane and it is on this plane most p-n junctions for LEDs are grown. Instead of reformation, chemical mechanical polishing (CMP) can be used to reshape the crystals from pyramid shape to the truncate pyramid shape. No matter which of these two methods that is used, the reshaped (In)GaN crystals can be used as dislocation-free substrates for growth of LEDs [8].

A p-n junction, which can be used in an LED device can be synthesised by growing a thick n-doped InGaN layer on top of one of these platelets, which will act as one of the barrier layers. This barrier is followed by a thin layer of InGaN with higher In content and layer thickness giving states in the quantum well which will correspond to the desired emission wavelength. The emission wavelength is mainly determined by the band gap, but fine-tuned by the states in the quantum well and thus the thickness of the InGaN layer corresponding to the quantum well. Finally on the other side of the quantum well a p-doped InGaN barrier layer is grown, see Figure 2.6. It has been demonstrated that InGaN layers with In content up to 18% can be grown by this method [8].

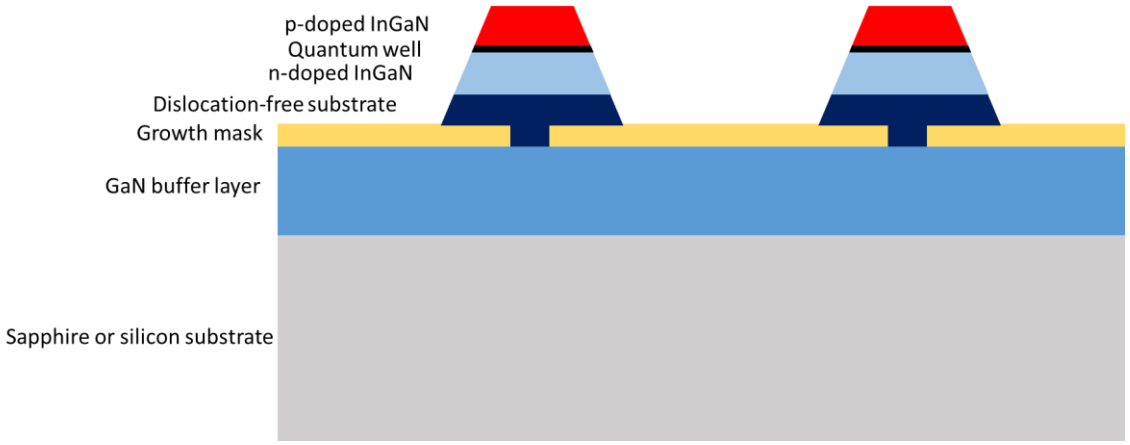

Figure 2.6
Structure of an InGaN platelet (dislocation-free substrate) with a p-n junction heterostructure grown on top. This structure has potential to be used in LED devices.

2.4 Previous LED device design based on InGaN and GaN platelets

In order to fabricate an LED based on the structure shown in Figure 2.6, one contact should be placed on the p-side and another contact should be placed on the n-side. The two contacts need to be isolated from each other, otherwise the LED would be short circuited. The previous process to do this is described in Figure 2.7. First a layer of Al_2O_3 is deposited using ALD (atomic layer deposition), then a spacer layer is spin-coated on top of the structure. By using RIE (reactive ion etch) the spacer layer is etched down so that the oxide layer on the p-side is exposed and then etched away in a wet etching process. The exposed p-side can then be contacted without contacting the n-side. A contact to the GaN buffer layer and thereby to the n-side is then made by applying a high voltage between the top contact and the substrate until a discharge occur.

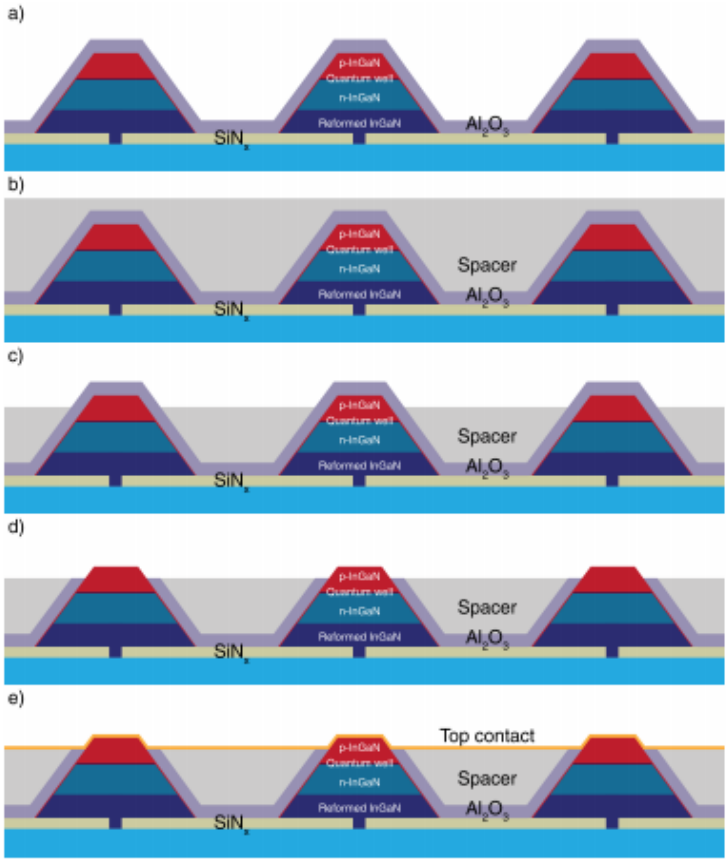

Figure 2.7

Figure describing the fabrication process of LEDs based on InGaN and GaN platelets.

- *a) Atomic layer deposition of Al_2O_3*
- *b) Spin-coating of spacer layer*
- *c) Etching of spacer layer in order to expose Al_2O_3 layer on the p-side of the platelets*
- *d) Etching of Al_2O_3 in order to expose the p-side*
- *e) Sputtering of a top contact on the p-side*

Adapted with permission from [6].

The device design shown in Figure 2.7 is not suitable for permanent connections by bonding and cannot be used to fabricate a packaged LED. The goal of this project is to develop an LED device design suitable for permanent connections by bonding in order to enable fabrication of a packaged LED demonstrator. In the next chapter the device design developed during the project is described.

3 Methodology

An LED device design suitable for permanent connections by bonding was fabricated, optimised and characterised. IV-characteristics and light output were measured for the samples, and an estimation of the EQE was calculated by comparing the light output power from a diode of known EQE with the light output power from the sample.

3.1 Growth of (In)GaN platelets

In this project the unprocessed samples consisted of a silicon or sapphire substrate with a thick layer of n-doped GaN, grown by metalorganic vapour-phase epitaxy (MOVPE). On top of this a growth mask of Si_3N_4 was deposited by low pressure chemical vapour deposition (LPCVD). These steps were done by an external supplier. At Lund University the sample was patterned by electron beam lithography (EBL). The pattern was then transferred to the growth mask by reactive-ion etching (RIE) of Si_3N_4. The resulting pattern consisted of hexagonal arrays of sub 100 nm openings in the growth mask. Short GaN nanowires were then grown by MOVPE in the openings of the growth mask. These nanowires were used as seeds for the following growth of (In)GaN platelets and finally p-n junction heterostructures were grown on top of the platelets. The platelets and p-n junctions on the samples in this project were grown by Taiping Lu and Zhaoxia Bi.

3.2 LED processing

The LED device design developed in this project is based on the design described in chapter 2.4. In order to enable permanent bonding the developed design has lifted bond pads, which gives stability and decreases the risk of shunt current to platelets outside of the device area. In the device area tens of thousands of platelets are connected to a transparent top contact of indium tin oxide (ITO), and the bond pad on the p-side is placed in an area that overlaps with the ITO but is outside of the device area. In order to get a contact to the n-side, an etching process is used to etch down to the GaN buffer layer, which enables deposition of a bond pad on the n-side.

The process steps for the first design are visualised in Figure 3.1, and the following chapters describes the optimisation of this design.

In the epitaxial growth of the platelets there is an abundance of hydrogen available and hydrogen atoms will therefore bond to the p-dopants (Mg), which becomes deactivated [5]. The first step was therefore to activate the p-dopants by rapidly increasing the temperature to 700 °C for 10 minutes under N_2 flow. This was performed using RTP-1200-100 from UniTemp GmbH. In this process the bonds between the p-dopants and hydrogen atoms will break and the p-dopants becomes activated. In next step an insulating layer of aluminium oxide was deposited using ALD system - Savannah-100. In the ALD process 200 cycles were performed at a temperature of 300 °C, which gave a thickness of approximately 20 nm. The thickness was estimated by measuring the thickness of the Al_2O_3 layer on top of a silicon reference using Ellipsometer, spectroscopic Woollam M2000VI. A spacer layer (S1805:PGMA 1:1) was then spin-coated on the sample at 3000 rpm for 60 s and permanent baked at 250 °C for 10 min. This spacer layer was then etched back using Etcher RIE - Trion T2 with 15 sccm O_2 flow at 300 mTorr and 50 W RF-power. In order to ensure that the polymer was etched back sufficiently to enable contact between the p-side of the platelets and the top contact (which is deposited in a later step) but not so far that the n-side becomes exposed, short etching periods were alternated with inspection in SEM - Hitachi SU8010. The oxide layer exposed was then etched by putting the sample in JTBaker BOE 10:1 for 40 s. A second spacer layer (S1813) was then spun on the sample at a rate of 3000 rpm for 60s. Then an opening for the device area (400x400 μm^2) was defined in the second spacer layer by soft UV-lithography using Mask aligner MJB4 and a dose of 210 mJ/cm^2. The resist was then developed using MF319 for 70 s. In next step a 100 nm thick layer of ITO (indium tin oxide) was sputtered in an area overlapping with the device area, and the p-side of platelets in the device area were thus connected to the top contact. The sputtered area was defined by a shadow mask. Deposition of the top contact was performed using Sputterer - AJA Orion 5. A bond pad on the p-side was then sputtered in an area outside of the device area but overlapping with the ITO top contact, the bond pad consisted of 5 nm Ti and 150 nm Au and the sputtered area was defined by a shadow mask. Next an etching process should be used to etch down to the buffer layer in order to enable deposition of a bond pad on the n-side, but for this first design a diamond pen was used to scratch down to the buffer layer. Finally the bond pad on the n-side was deposited in the scratched area using the same procedure as for the bond pad on the p-side.

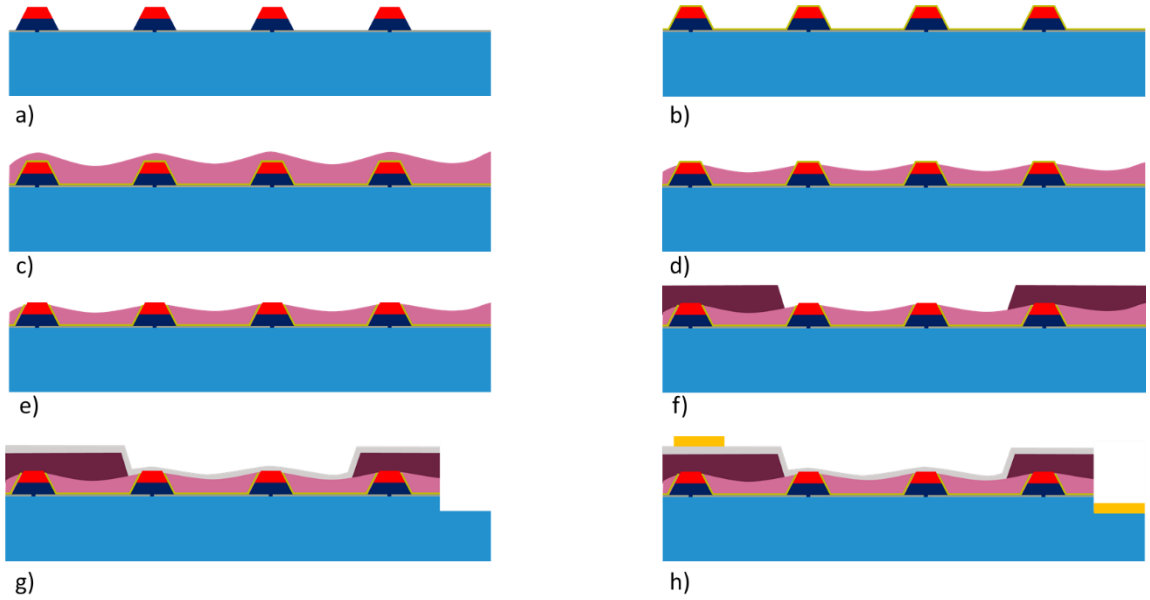

Figure 3.1
Sketches of the different process steps in fabrication of the device. The thick light blue layer corresponds to the GaN buffer layer and the thin grey layer corresponds to the Si_3N_4 growth mask. The red and dark blue layers correspond to the p- and n-barriers respectively.

- *a) RTP (700 °C, 10 min)*
- *b) ALD (200 cycles Al_2O_3)*
- *c) Deposition of spacer layer 1 (S1805:PGMA)*
- *d) Etch back using O_2 plasma*
- *e) BOE etching of Al_2O_3*
- *f) Deposition of spacer layer 2 (S1813) and definition of opening (device area) using UV-lithography*
- *g) Deposition of top contact and etching to GaN buffer layer (scratching with a diamond pen)*
- *h) Deposition of bond pads (Ti/Au) in areas defined by a shadow mask*

3.3 Characterisation

IV-characteristics and light output were measured for the samples using Probe station - Cascade 11000B and a spectrometer, see Figure 3.2. One probe was placed on the bond pad on the n-side and the other probe was placed on the bond pad on the p-side, then a voltage sweep was performed and the current measured. In order to measure the light output, the sample was enclosed in a cavity blocking light from surroundings and a constant voltage was applied to the sample while the light output was measured by the spectrometer. The EQE for the samples was calculated by comparing the light output power from a diode of known EQE with the light output power from the sample.

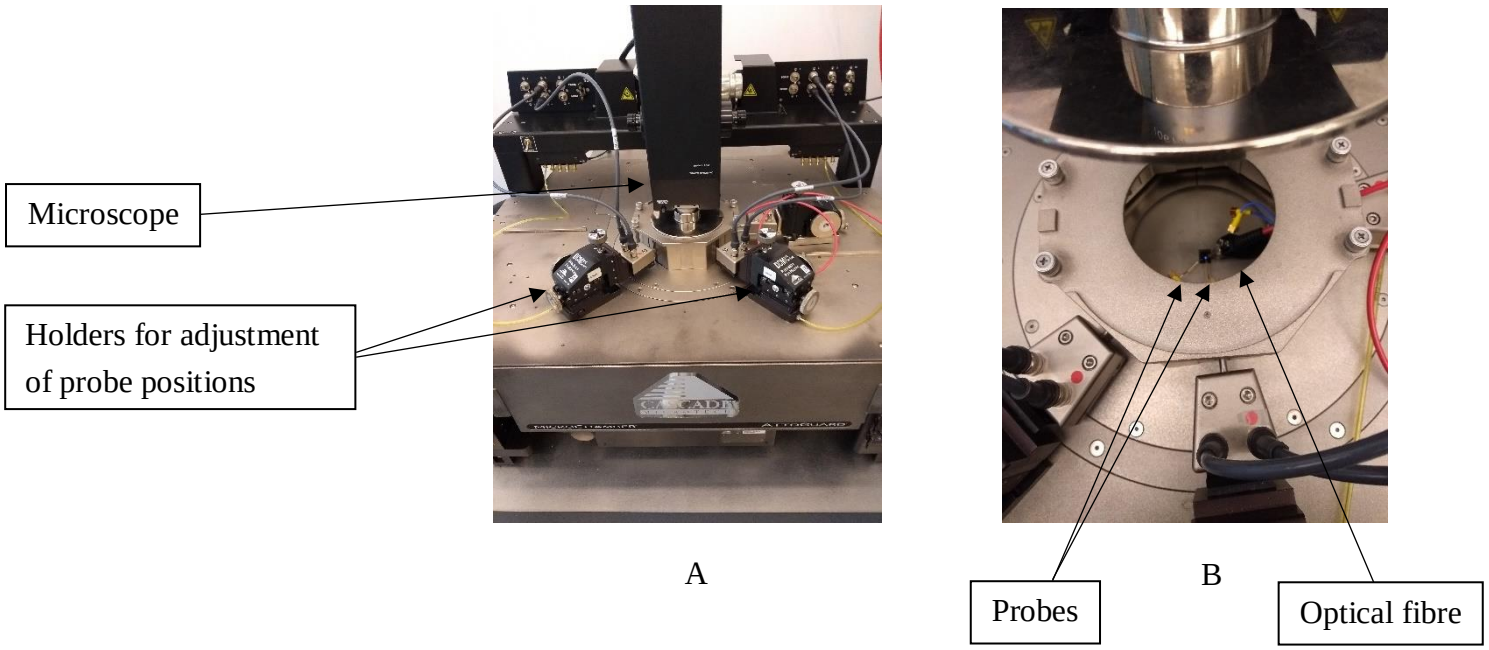

Figure 3.2

A) Image showing the setup used when measuring the light output. The sample is enclosed in a cavity in order to block light from surroundings.

B) Image showing a sample inside the cavity. Two probes are placed on the respective bond pads and to the right the optical fibre is shown.

4 Results and discussion

In this chapter the results from processing and characterisation are shown and discussed.

4.1 First device

Figure 4.1 shows the platelets after etch back of spacer layer 1 (A) and after etching of the oxide layer on top of the platelets (B), and Figure 4.2 shows the first device during measurements.

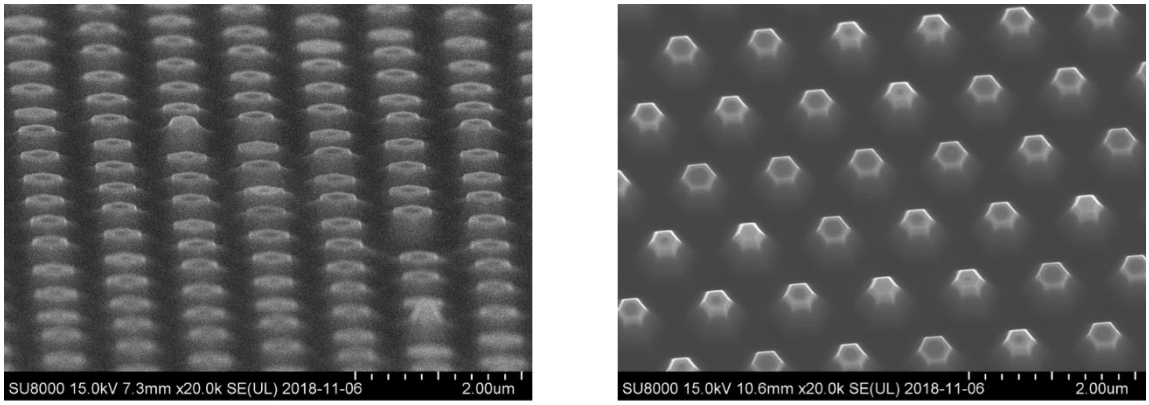

Figure 4.1

A) *SEM image showing the platelets after 30 s etch back of spacer layer 1. It is clear that the top of the platelets are free from resist, which enables etching of the oxide layer on top of the platelets.*
B) *SEM image showing the platelets after 40 s wet etching with BOE 1:10. It is hard to see if the oxide layer has been etched but it looks like the platelets have sharper edges compared to before the etching, see A), which is an indication that the oxide layer has been etched.*

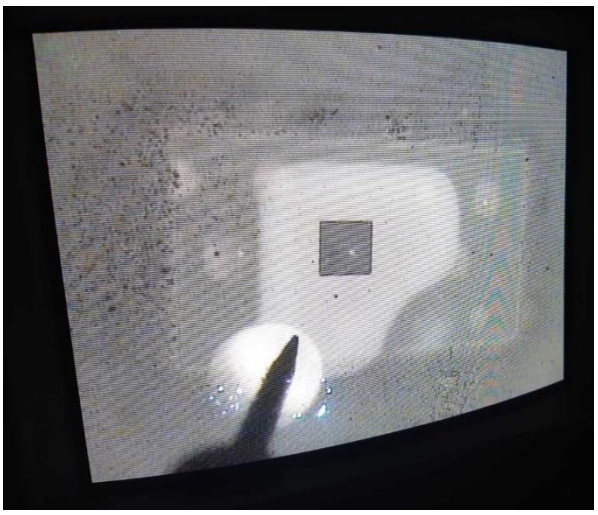

Figure 4.2
Image showing the sample during constant applied voltage. The large rectangle in the image corresponds to the area where platelets are grown and the small dark square in the centre of this area corresponds to the device area. The large square with a cutout corresponds to the top contact and the circle in bottom left of the top contact corresponds to the bond pad on the p-side. The platelets in the device area (small dark square) do not light up but instead some parasitic grown crystals outside of the area where platelets are grown light up. Small circles are also visible in the area where platelets are grown, which correspond to Ni deposition from a previous processing (this sample has been processed twice).

In Figure 4.2 the main problem with this first sample is clearly shown. No platelets in the device area light up but instead some tall parasitic grown crystals outside of the area where platelets are grown light up. The reason is probably that these parasitic grown crystals have a height above spacer layer 2, and therefore there is a leakage of current to these platelets so that almost no current reaches the platelets in the device area. In order to solve this problem a thicker resist was used as spacer layer 2 in the following designs.

Another drawback with this device design is that the oxide etching was performed before deposition of the second spacer layer which enables for possible leakage to platelets outside of the device area, see Figure 4.3. Of course it would be much better to etch down to the GaN buffer layer instead of scratching with a diamond pen.

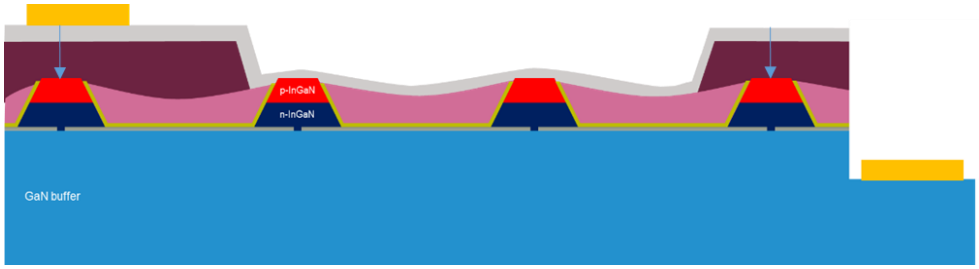

Figure 4.3
Blue arrows indicating possible leakage current in the first device design.

4.2 Optimisation of spacer layer thickness and development of etching process to GaN buffer layer

To solve the leaking problems associated with the first device design the oxide etching was postponed to after definition of the openings in spacer layer 2, which was also made thicker. The oxide layer was also made thicker (400 cycles) approximately 40 nm, to further ensure no leakage current and to protect the p-doped side of the platelets from incorporation of oxygen during oxygen plasma etching. Incorporated oxygen, creates a deep level trap and counteract the p-dopants which leads to lower doping and thus lower concentration of free charge carriers [20]. Due to the thicker oxide layer the oxide etching was performed for 80 s instead of 40 s. A real etching process was also used instead of scratching with a diamond pen. The process steps are visualised in Figure 4.4.

An opening for the n-contact was defined already in spacer layer 1 (S1805:PGMA 1:1) and then also in spacer layer 2 (S1828). After deposition of the ITO top contact an etch mask (S1813) was spin-coated on the sample at a rate of 3000 rpm for 60 s, and an opening for the n-contact was defined by UV-lithography. The etch mask was not post-baked in order to be able to remove it in a later process step. The growth mask (Si_3N_4) was then etched using Etcher RIE - Trion T2 with a CHF_3 flow of 10 sccm at 50 mTorr and 75 W RF-power. The process time for etching of the growth mask was 500 s. Then the etch mask was stripped by putting the sample in Remover 1165 for 30 min at a temperature of 90 °C. Finally the bond pads on the p-side and n-side were deposited. Figure 4.5 shows a finished device.

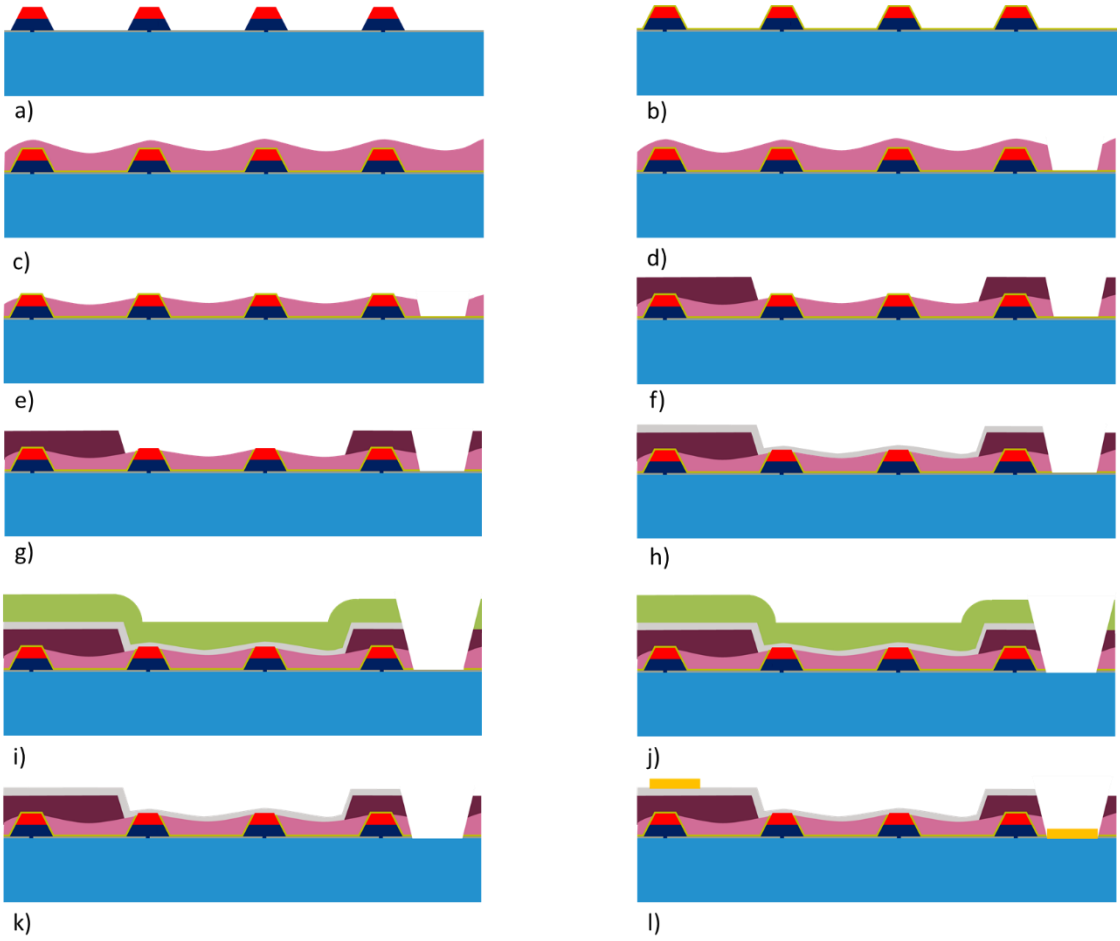

Figure 4.4

Sketches of the different process steps in fabrication of the device. The thick light blue layer corresponds to the GaN buffer layer and the thin grey layer corresponds to the Si_3N_4 growth mask. The red and dark blue layers correspond to the p- and n-barriers respectively.

- *a) RTP (700 °C, 10 min)*
- *b) ALD (400 cycles Al_2O_3)*
- *c) Deposition of spacer layer 1 (S1805:PGMA 1:1)*
- *d) Definition of opening in spacer layer 1 by UV-lithography. The opening corresponds to the area where the n-contact will be*
- *e) Etch back of spacer layer 1 using O_2 plasma*
- *f) Deposition of spacer layer 2 (S1828) and definition of openings for the device area and for the n-contact*
- *g) BOE etching, which removes the oxide layer on top of the platelets in the active area as well as in the area defined for the n-contact*
- *h) Deposition of top contact (ITO) in an area defined by sputtering through a shadow mask*
- *i) Deposition of etch mask (S1813) and definition of opening for n-contact*
- *j) Etching of growth mask (RIE CHF_3)*
- *k) Stripping of etch mask using Remover 1165*
- *l) Deposition of bond pads (Ti/Au) in areas defined by a shadow mask*

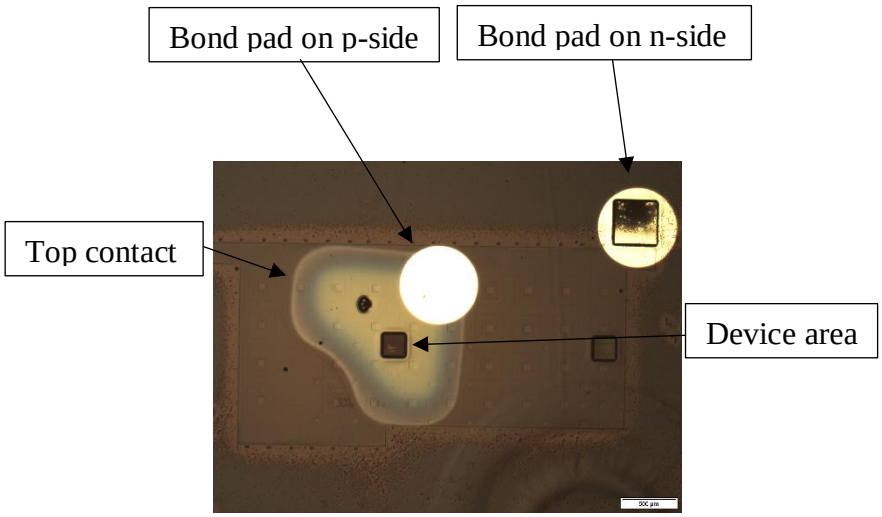

Figure 4.5
Image showing a finished device. The large rectangle corresponds to the area where platelets are grown, and the other parts of the sample are indicated by arrows.

Figure 4.6 gives a hint of the main problem of this design. It is shown that only the tallest platelets light up. The first assumption was therefore that spacer layer 1 was not etched sufficiently to enable etching of the oxide layer and contact between the top contact and the p-side of the platelets. But after inspection of cross-sections of the n-contact and the device area (see Figure 4.7 and 4.8, respectively), it is clear that the main problem is that a thin layer of resist remains in the UV-lithography defined areas after development. This thin layer has covered the platelets in the device area so that the oxide layer on top of the platelets has not been etched. Therefore only platelets with a height above this layer have got their oxide layer etched and been connected to the top contact, which is the reason why only the tallest platelets light up.

Figure 4.6
Image showing the device area while a constant voltage is applied. Only platelets around parts of the platelet array where no platelets are grown light up and these platelets usually tend to be slightly taller than the average platelet. The emission in the bottom left of the image is probably due to recombination over the bandgap of GaN, which gives light of a shorter wavelength.

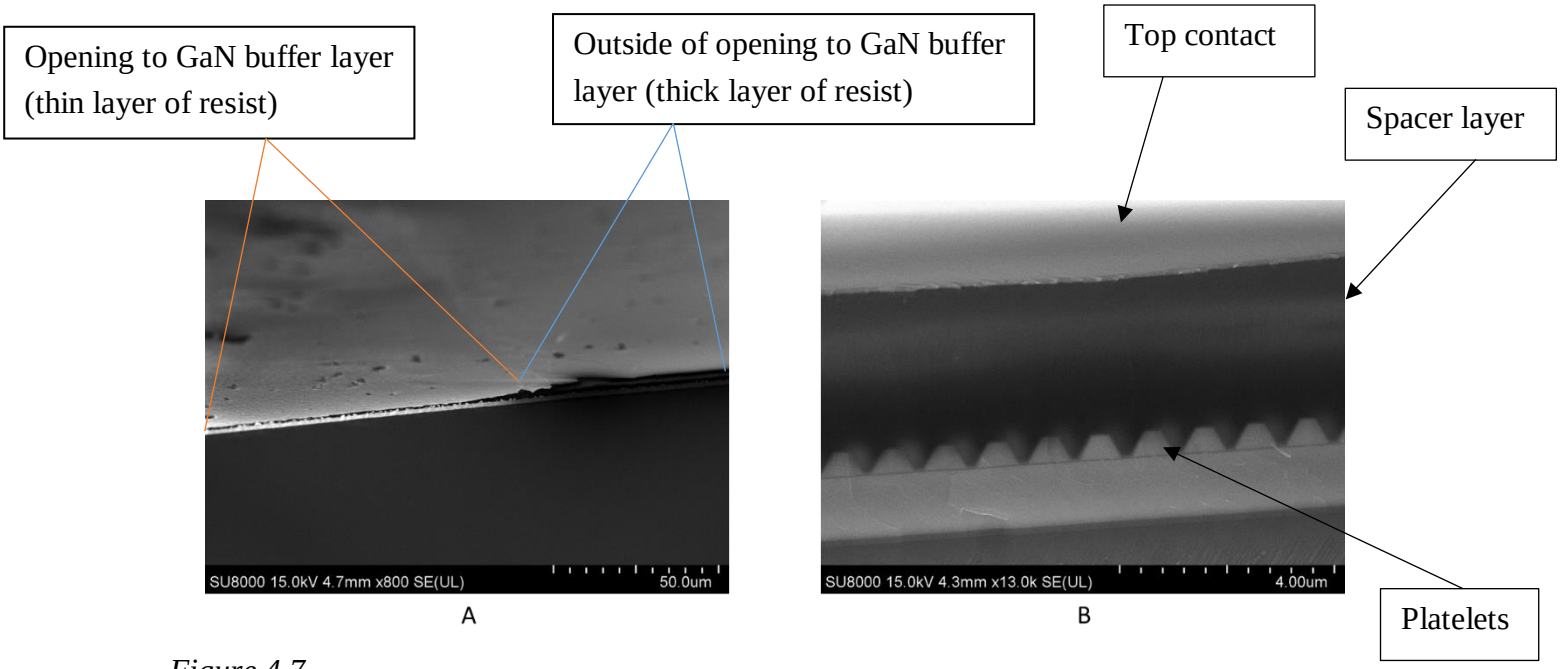

Figure 4.7
SEM-images showing cross-sections after cleavage of a sample.

- *A) Cross-section of the n-contact after cleavage of the sample. The slope profile of the spacer layer is clearly visible as well as an unwanted thin layer of resist in the opening to the GaN buffer layer.*
- *B) Cross-section of the platelet array outside of the device area. It is clear from the image that the resist layer is thick enough to cover the platelets.*

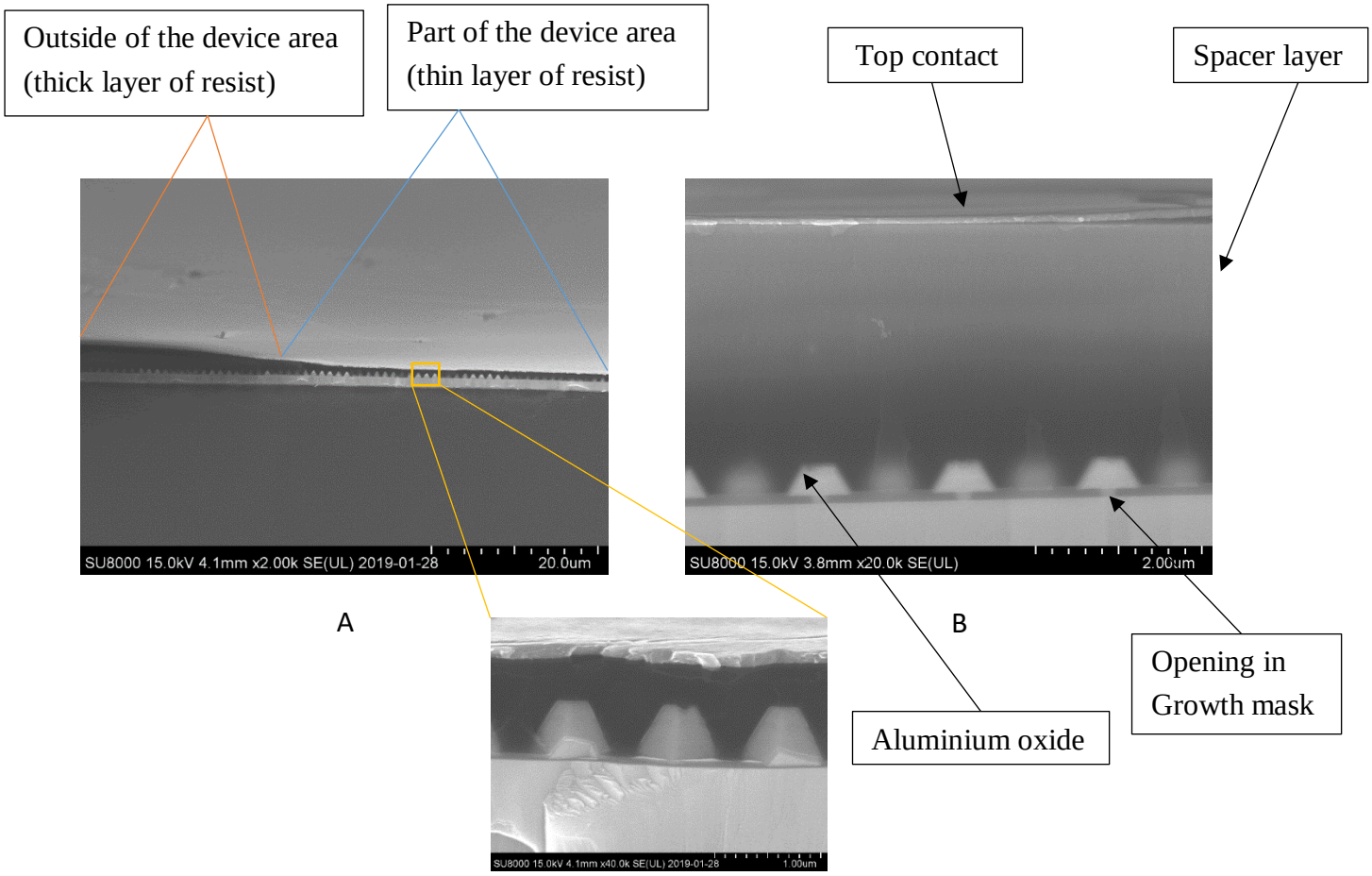

Figure 4.8

A) SEM-image showing a cross-section of the device area. It is clear from the image that there is a thick resist layer covering the platelets outside of the device area (left part of the image), but the platelets in the device area totally covered by resist (right part of the image).

B) SEM-image showing that the platelets outside of the device area are covered by a thick layer of resist. It is also possible to see the openings in the growth mask as well as the aluminium oxide layer covering the platelets.

By increasing the exposure dose (500 mJ/cm^2) and using a longer development time (150 s) for spacer layer 2 (S1828), more platelets light up (enough platelets in order to be able to measure the light output). At low voltage only some platelets around areas in the platelet array where no platelets are grown light up (tallest platelets), but at higher voltage more and more platelets light up. The conclusion is that there probably still is resist covering the platelets but the layer is thinner, and therefore more platelets have a height above the resist and thus light up. One possible explanation to why more platelets light up when a higher voltage is applied, is that some platelets may be partly covered by a thin layer of resist and the oxide layer on these platelets has therefore not been completely etched away, which gives rise to a higher resistance

and therefore a higher voltage is needed in order to get the platelets to light up. In Figure 4.9 the IV-characteristics for a device consisting of 160 000 platelets is shown and Figure 4.10 shows Electroluminescence (EL) spectrum for different current densities. The calculated EQE is low.

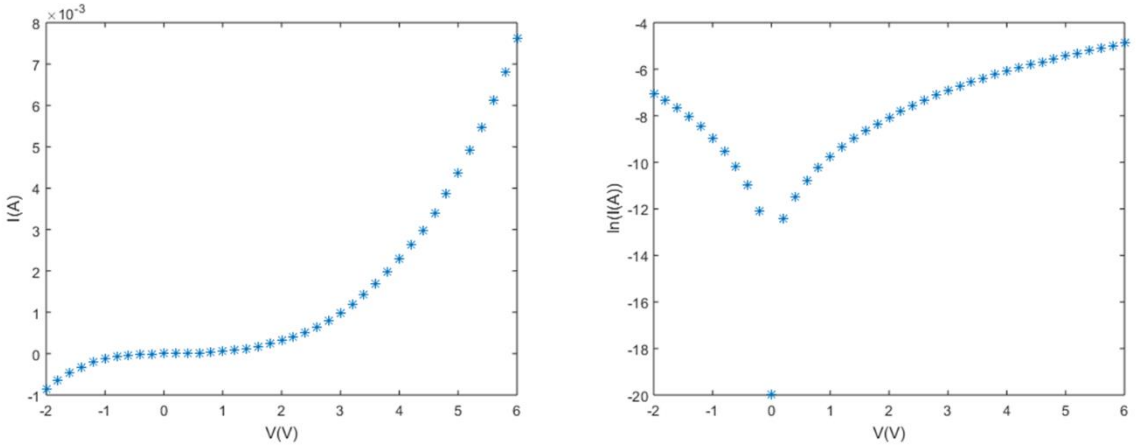

Figure 4.9
The device shows no rectification and the current does not depend exponentially on the voltage, which it should for a diode, see eq (2.1).

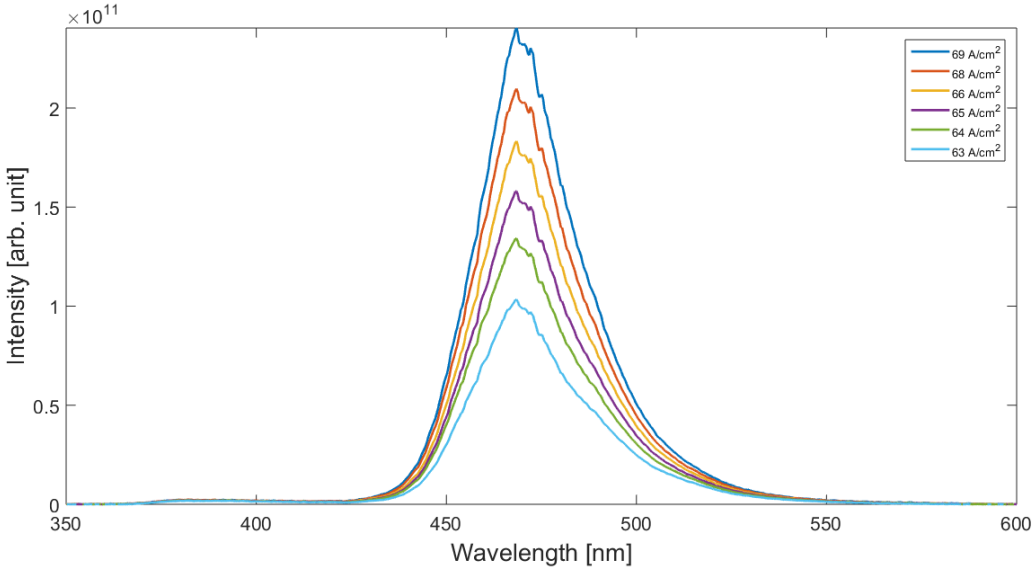

Figure 4.10
Spectrum of the light output at different current densities. The emission due to recombination in the quantum well dominates and the emission peak is at 468 nm. A small peak is also visible at about 385 nm, which corresponds to recombination outside of the quantum well.

In order to get rid of all resist residues in the UV exposed areas of spacer layer 2 the oxygen plasma etching step was postponed to after definition of the openings in spacer layer 2. Now most of the platelets in the device area light up and the etched n-contact could be used (instead of the backside of the silicon substrate, which has been used for some of the previous samples), which indicates that all resist residues are gone. The oxide layer and growth mask in the area of the n-contact has therefore been etched, resulting in a much better n-contact. And most of the platelets in the device area has got their oxide layer on the p-side etched, which is the reason why most of the platelets light up and not only the tallest. Figure 4.11 shows IV-characteristics for a device consisting of 40 000 platelets. The results look in principle the same as for a device consisting of 160 000 platelets. No current rectification is shown, the current does not depend exponentially on the voltage and the EQE is very low. In Figure 4.12 it is shown that all platelets does not light up at the same time. Figure 4.15 shows the EL spectrum and Figure 4.16 shows two samples while recording the EL data. In the EL spectrum a peak corresponding to emission from parasitic grown crystals in the device area is visible (at 407 nm). The reason why this peak is not visible in previous EL spectrum is that this specific sample contains more parasitic grown crystals than previous samples (epitaxy related problem).

One possible explanation of the results is that in the device area there are some parasitic grown crystals which are much taller than the platelets (see Figure 4.12, Figure 4.13 and Figure 4.14) and therefore both the p-side and n-side of these crystals are connected to the top contact, which results in by-passing of the p-n junction and a linear dependence between current and voltage

(and non-rectifying behaviour). The overall dependence should therefore be somewhere in between linear and exponential which corresponds well to the IV-curves, see Figure 4.9 and Figure 4.11. The low external quantum efficiency (EQE), can probably also be explained by tall parasitic grown crystals in the device area and by-passing of the p-n junction.

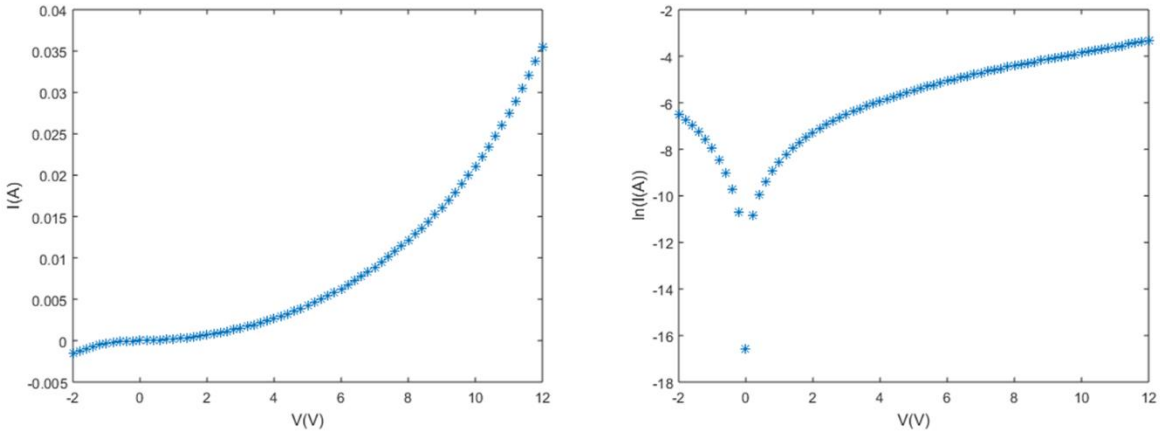

Figure 4.11
IV-curve, showing that the current does not depend exponential on the voltage, and the current is in principle the same in both forward and reverse direction.

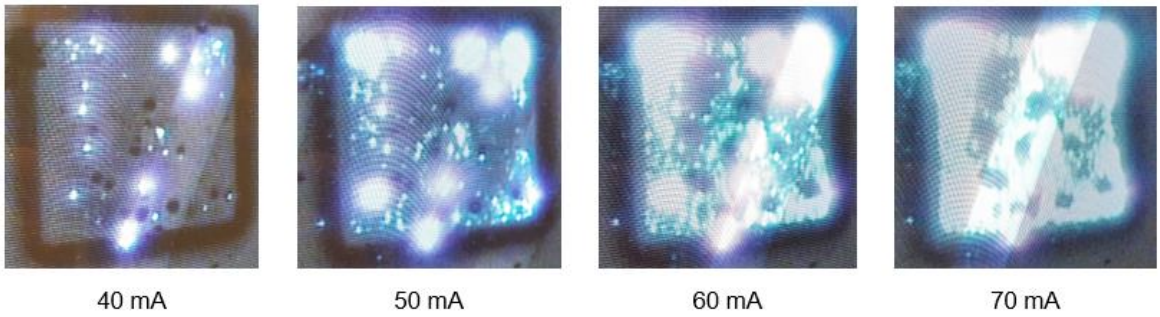

Figure 4.12
Images of the device area for some different currents. For low current some of the big parasitic grown crystals light up, and then at higher current more and more of the platelets light up. At 70 mA most of the platelets in the device area light up except for some dark areas around big parasitic grown crystals which probably is due to bunching of the resist and the platelets in these areas are thus covered by resist. The bright diagonal line is an artefact from the image capture.

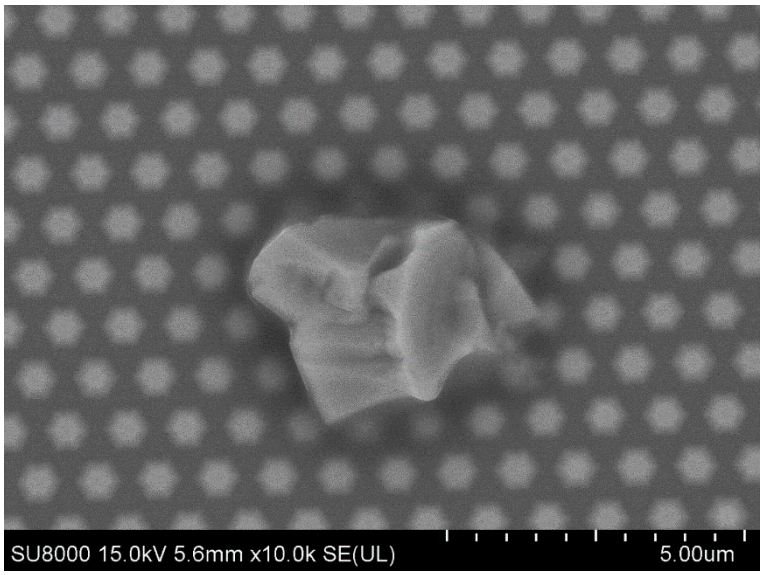

Figure 4.13
SEM-image showing a parasitic grown crystal in the device area, before etch back of the spacer layer. All platelets are covered by resist but the parasitic grown crystal, which is much taller than the platelets protrudes from the resist. Also note the irregular shape of the parasitic grown crystal.

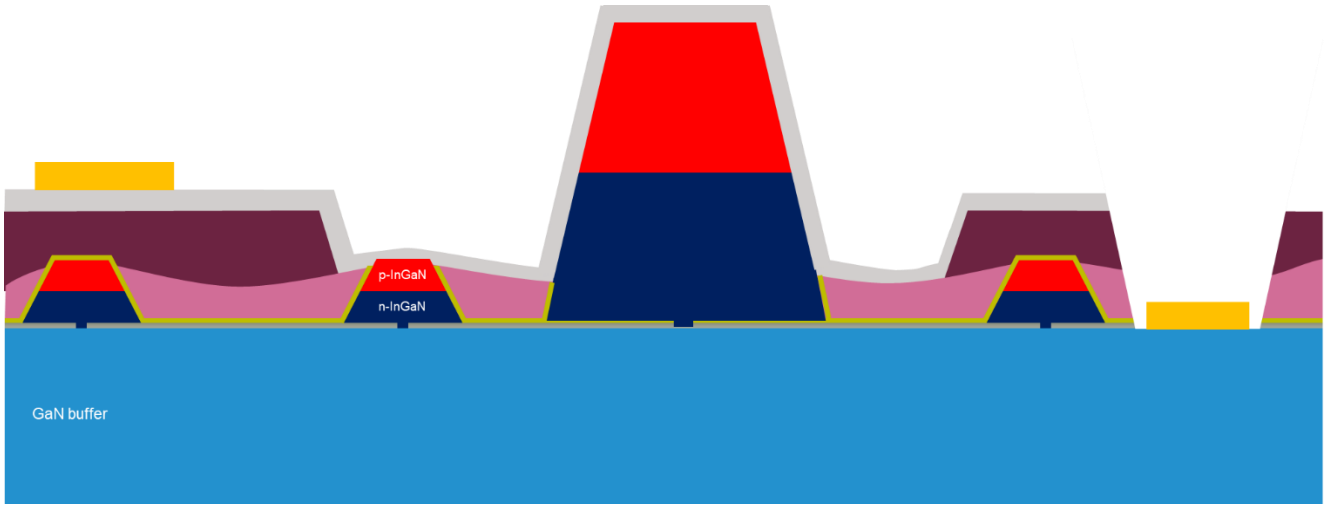

Figure 4.14
Sketch showing a parasitic grown crystal in the device area. Both the p-side and the n-side of the crystal are connected to the top contact, which results in by-passing of the p-n junction and a linear dependence between current and voltage. In this sketch the parasitic grown crystal has the same shape as the platelets but in reality the shape is irregular (see Figure 4.13).

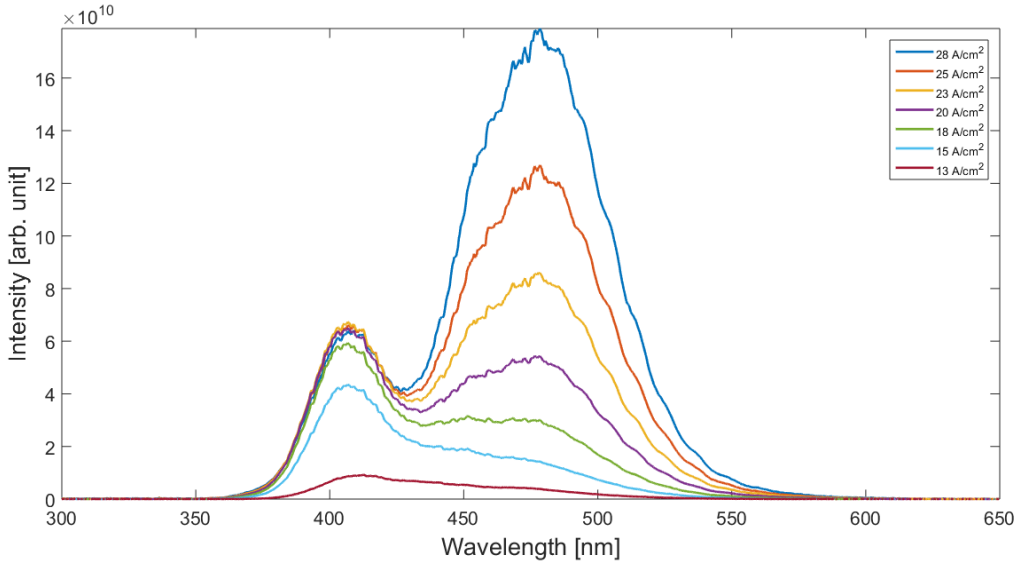

Figure 4.15
Spectrum of the light output for different current densities. At low current density the emission peak at 407 nm dominates but at higher current density the two (overlapping) emission peaks at 450 and 477 nm become dominating. Since some big parasitic crystals light up first and then more and more of the platelets, the emission at shortest wavelength corresponds to emission from parasitic grown crystals and the other two peaks correspond to emission from the platelets.

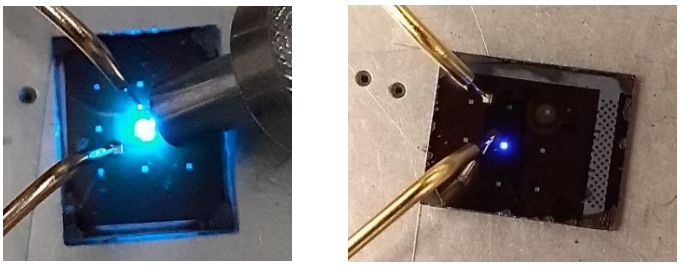

A B

Figure 4.16
Image of two samples (both consisting of 40 000 platelets) during recording of EL spectrum. To the left the two probes are shown and to the right the optical fibre (not shown in image B) which is connected to the spectrometer is shown. The light output looks much brighter from the sample grown on sapphire substrate (A) compared to the light output from the sample grown on silicon substrate (B). EQE and IV-characteristics look similar for both samples and most of the platelets in respective device area light up. The difference in brightness could be due to more absorption in the silicon substrate compared to the sapphire substrate.

4.3 Back contact

The processing would require fewer steps if the same contact materials could be used for both the top and back contact. By measuring the current between pairs of contacts to the GaN buffer layer, consisting of Ni/ITO and Ti/Au, it is shown that the back contact will be much worse if the same material as the top contact (Ni/ITO) is used. The contact is not ohmic and the resistance is very high, see Figure 4.17 A-B. By using the originally intended back contact (Ti/Au) the resistance is lower and an ohmic behaviour is seen, see Figure 4.17 C-D. The reason is probably that the work function (difference between vacuum energy and fermi level) of n-doped GaN is more similar to the work function of Ti than to the work function of Ni giving less band bending in the interface between semiconductor and metal (and therefore lower resistance and a more linear behaviour between current and voltage) [21].

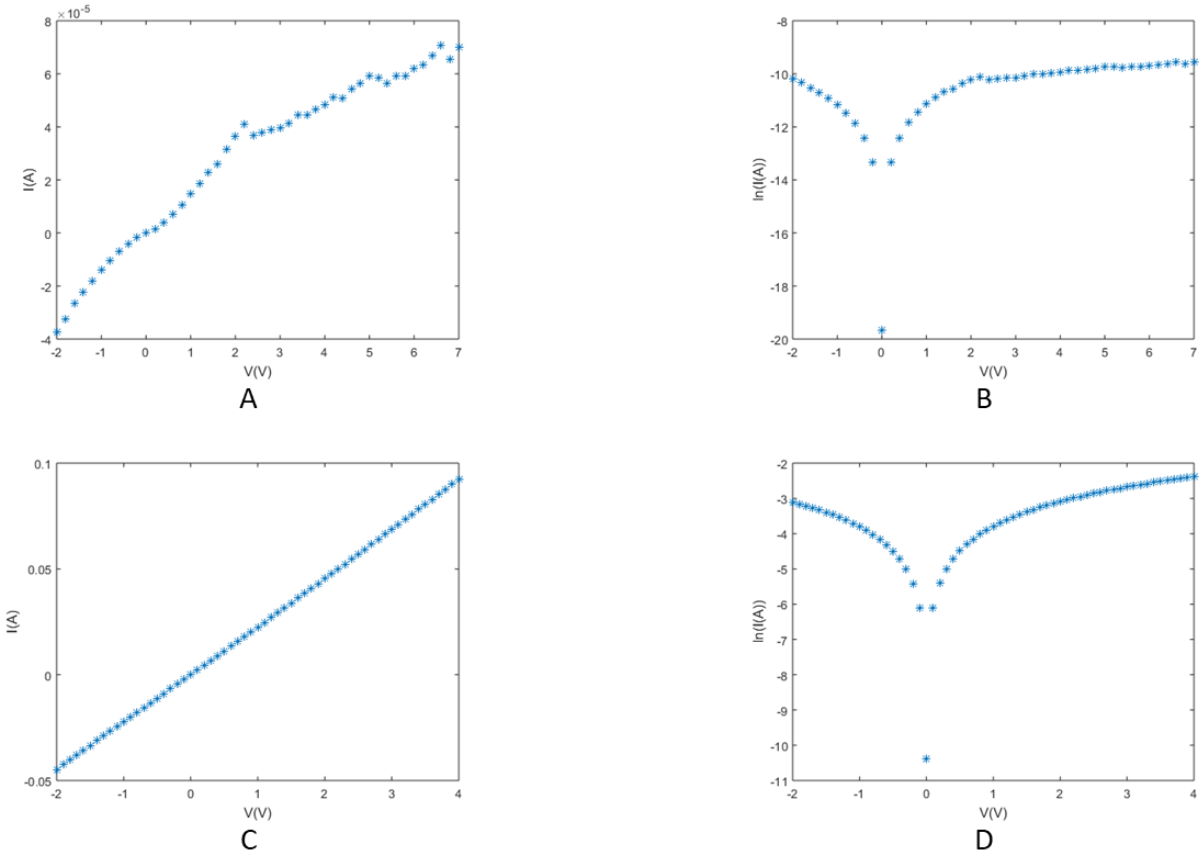

Figure 4.17
Graphs showing the IV-curves for the different types of back contacts.
A-B) Voltage is applied between two Ni/ITO back contacts.
C-D) Voltage applied between two Ti/Au back contacts.

4.4 Top contact

One of the greatest challenges with this design is to contact all platelets in the device area to the top contact and at the same time avoiding short-circuiting of any platelets. This requires very good uniformity in the growth of the crystals and spacer layers of uniform thicknesses. But even if these requirements are fulfilled it is important that the quality of the top contact is good (high transmittance, low resistance and ohmic behaviour).

The resistivity ($\rho = R\frac{A}{L}$) of the Ni/ITO contact was investigated by defining pairs of bond pads and connections between each pair using Raith Voyager, see Figure 4.18. Ni/ITO (3 nm/75 nm) was then sputtered on the sample and unwanted metal deposition was removed in the following lift-off.

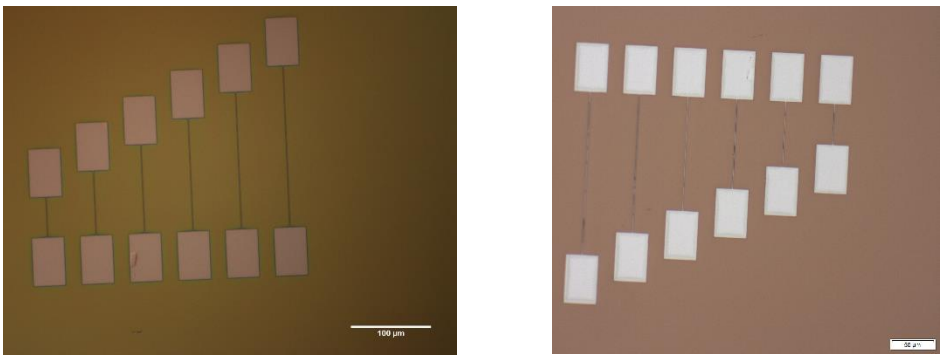

A B

Figure 4.18

Images showing the EBL-defined structures used in investigation of the resistivity of Ni/ITO contacts. Image A is before deposition of the metal and B is after lift-off with Remover 1165.

By measuring the resistance between the bond pads when 1 V was applied and then plotting the resistance versus the length of the connection between the bond pads, the slope of a linear regression gives a value of resistance per length. If this value is multiplied by the cross-section area of the connection, a value of the resistivity is obtained. In Figure 4.19 the slope is $1{,}2 \cdot 10^{8}$ Ω/m, and the cross-section area is $7{,}8 \cdot 10^{-14}$ m^2 , which gives a resistivity of $\rho = 9{,}4 \cdot 10^{-6}$ Ωm. This estimated value of the resistivity is in the expected order of magnitude [22].

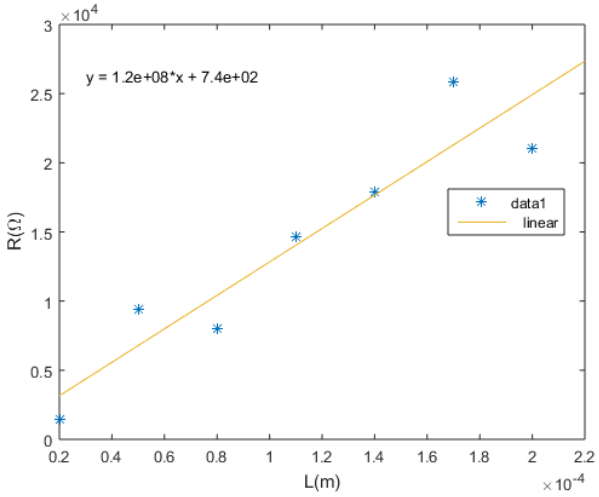

Figure 4.19

The resistance between the bond pads when 1 V was applied as function of distance between the bond pads. A linear regression to the data points is included.

4.5 CMP-samples

In order to reduce the number of tall parasitic grown crystals and bypassing of the p-n junction, devices based on platelets reshaped by CMP (see chapter 2.3) were fabricated. Figure 4.20 and 4.21 show the platelets in the device area after O_2 plasma etching and BOE respectively.

Still all platelets do not light up at the same time (see Figure 4.23), but a difference compared to the samples reshaped by reformation is that the emission is more uniform and in principle all platelets in the device area light up. For samples reshaped by reformation dark areas around big parasitic crystals can be shown, which is not visible for the CMP samples. Compare for instance Figure 4.12 (reshaped by reformation) and Figure 4.23 (reshaped by CMP). The conclusion is that the CMP-samples contain less big parasitic crystals and the platelets have more uniform height. IV-characteristics and EQE look similar to previous devices (reshaped by reformation, see chapter 2.3). The devices show not an exponential dependence between current and voltage and no rectification, see Figure 4.22. Figure 4.24 shows a sample emitting in the red region and Figure 4.25 shows the corresponding EL spectrum.

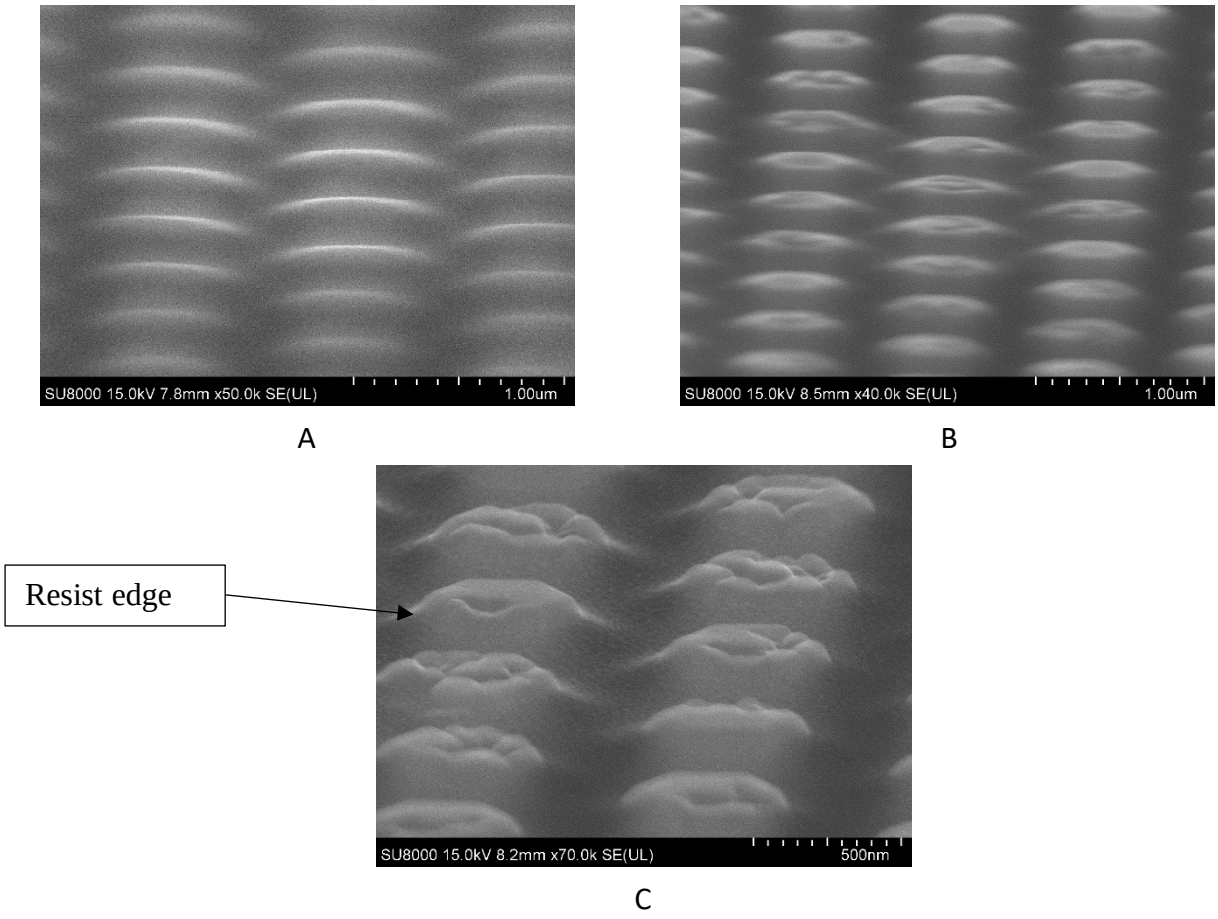

Figure 4.20

Images showing the platelets in the device area after oxygen plasma etching for different times.

- *A) Oxygen plasma etching for 90 s. The platelets are totally covered by resist*
- *B) Oxygen plasma etching for 285 s. The platelets are probably still totally covered by resist but it is possible to see that the surface on top of the platelets are rough. This roughness was not seen on the other samples and the reason is that the p-InGaN layer on this sample was grown with a higher growth rate compared to previous samples.*
- *C) Oxygen plasma etching for 345 s. About 70 nm of the platelets are free from resist, and 40 nm of this corresponds to the thickness of the aluminium oxide covering the platelets. This should be enough etching to enable good contact between the p-side of the platelets and the top-contact without short-circuiting the platelets.*

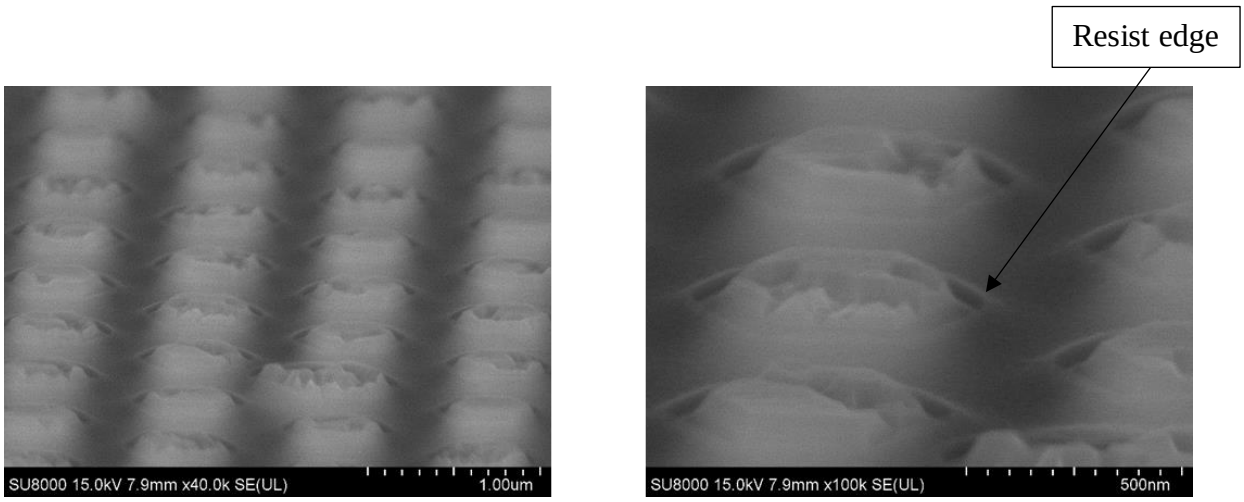

Figure 4.21
SEM-images of platelets in the device area after 80 s BOE. By comparing these images with image C in Figure 4.20 it is clear that the edges of the platelets are sharper after 80 s BOE, which is an indication that the oxide layer has been etched. Another difference is that there is a gap between the resist and the platelets after BOE, which is due to absence of the oxide layer.

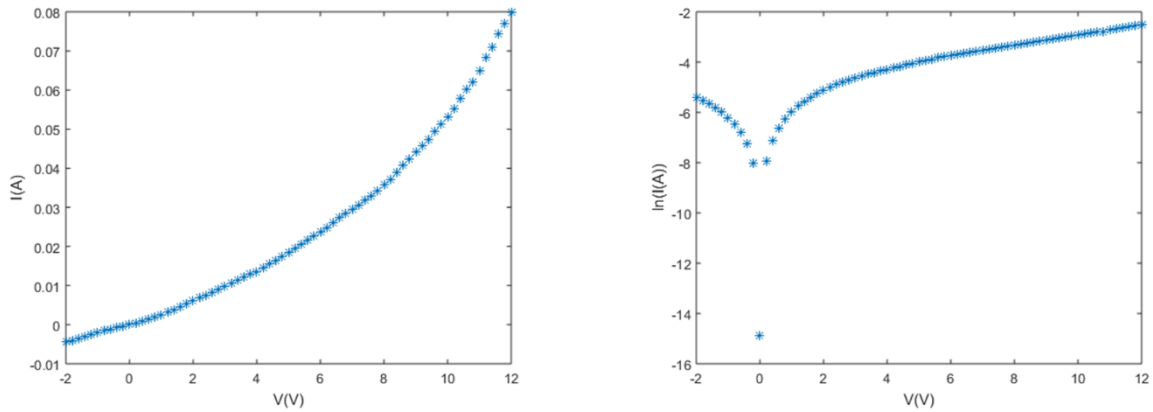

Figure 4.22
IV-curve showing that the current does not depend exponentially on the voltage which it should for a diode, and no noticeable rectification is shown.

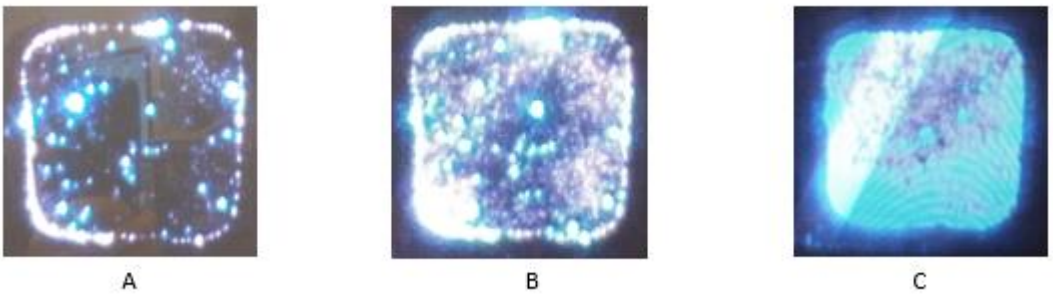

Figure 4.23
Images of the device area for different applied voltages. At low voltage only some platelets light up and then when the voltage is increased more and more platelets light up, and for 12 V in principle all platelets in the device area light up (image C) indicating good homogeneity in the physical contact between the ITO and the crystals. The darker area of the device area in image C is probably because of a layer of by-products formed during etching for the back contact, which has not been removed in the lift-off. The layer is probably thicker in this area which is the reason why it looks darker (less light travels through the layer).

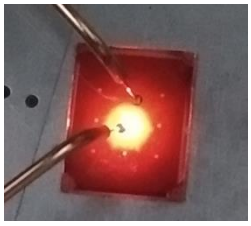

Figure 4.24
Image showing that the emission from this sample is in the red region. On the screen showing the device area it looked like the emission was in the blue region (Figure 4.23), which is due to the sensitivity of the CCD camera.

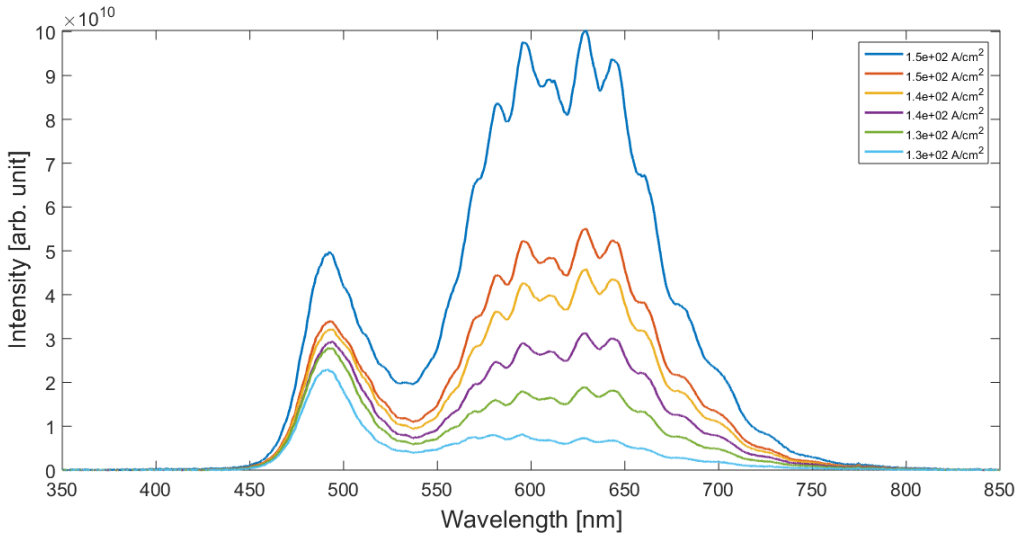

Figure 4.25

Spectrum of the light output at different current densities. At low current density the emission peak at 492 nm dominates but at higher current density a broad emission peak at 625 nm becomes dominating. The features on the broad emission peak could be due to Fabry–Pérot interference, due to light reflected at the interface between the GaN buffer layer and the substrate and at the interface between the top of the platelet and the top contact. The peak at 492 nm probably corresponds to emission over the bandgap of p-doped InGaN and the broad peak corresponds to emission over the quantum well.

Since these samples were reshaped by CMP the platelets should have a much more uniform height and the number of tall parasitic grown crystals should be much less than for the previous samples which were reshaped by reformation. So why do we still have bad IV-characteristics and low efficiency? An explanation could be, due to inhomogeneity in thicknesses of the barrier layers and quantum wells as well as inhomogeneity in resist thicknesses. Inhomogeneity in c-plane areas will lead to different thicknesses of the layers and the total height will therefore be different (see Figure 4.26), which leads to different contact areas to the top contact (some platelets may also be short-circuited). Because of the different thicknesses of the p-layer the voltage drop over the p-side will vary and maybe also the threshold voltage, which may explain why all platelets do not light up at the same time (Figure 4.23).

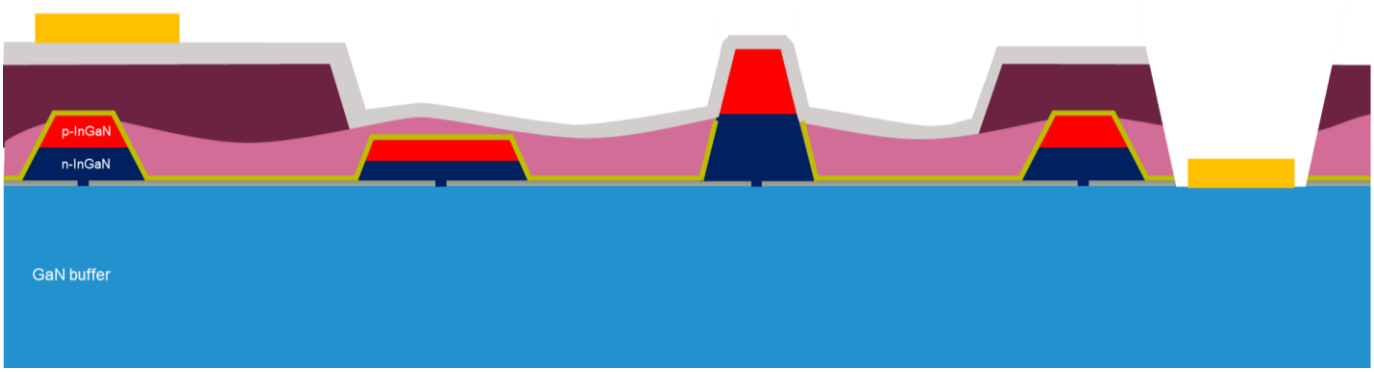

Figure 4.26
Sketch showing a possible explanation to the low efficiency and bad IV-characteristics. Variations in c-plane areas give rise to different thicknesses of the barrier layers and quantum wells, which in the end gives a variation in height between the crystals. In the sketch an unusual tall platelet and an unusual short platelet are shown. The short platelet is not connected to the top contact and will thus not emit any light. For the tall platelet on the other hand, both the p-side and n-side is connected to the top contact. The p-n junction is therefore by-passed which gives a non-rectifying behaviour and a linear dependence between current and voltage.

4.6 Investigation of crystal homogeneity by fabrication of different device sizes

Even though CMP-samples are used the devices show low efficiency and no rectification. In order to investigate if this has to do with inhomogeneity in thicknesses of the barrier layers, quantum wells and resists, different device sizes were fabricated and compared.

Raith Voyager was used to expose squares corresponding to devices of different sizes (400 μm^2, 100 μm^2, 25 μm^2, 4 μm^2 and 1 μm^2) in the device area defined in spacer layer 1. Since the pitch was 1 µm the devices consisted of 400, 100, 25, 4 and 1 platelet respectively. An acceleration voltage of 50 kV and a dose of 500 $\mu C/cm^2$ were used and after exposure the resist (950 PMMA A6) was developed in MIBK(methyl isobutyl ketone):IPA 1:3 for 90s and then put in IPA for 20 s. The oxide layer on top of the platelets in the areas defined by EBL was then etched by putting the sample in JTBaker BOE10:1 for 80s. The e-beam resist was then stripped by putting the sample in acetone for 60 min and then in IPA for 1 min. A new layer of 950 PMMA A6 was then spin-coated on the sample. Raith Voyager was then used (using the same settings as before) to expose the squares corresponding to the devices but also areas for the contacts, see EBL design in Figure 4.27. The bond pad in the top left of Figure 4.27 B was not connected to any device in order to be used as a reference structure for measuring the leakage current through the spacer layers ($3 \cdot 10^{-14}$ A at 7 V).

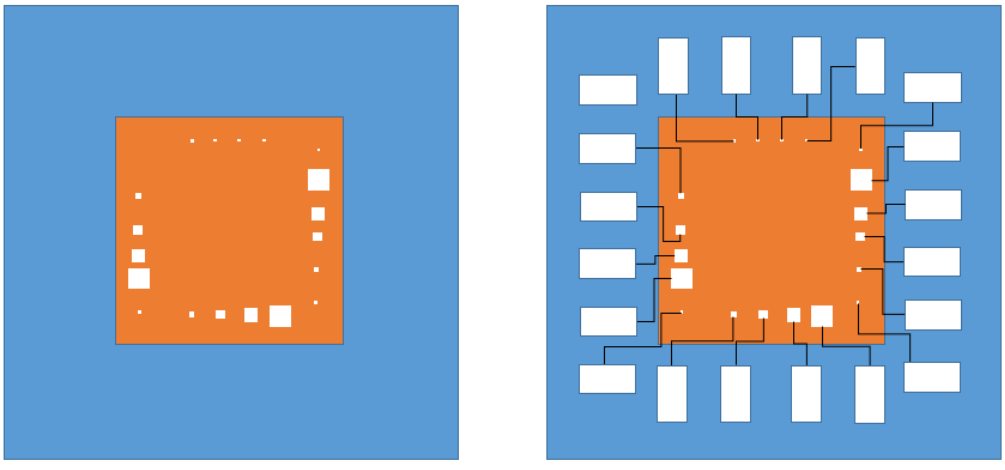

Figure 4.27

Sketches showing the areas defined by EBL. The blue square corresponds to the write field (400 µm x 400 µm) and the red square corresponds to the UV-lithography defined opening in spacer layer 1 (200 µm x 200 µm).

A) First only the squares corresponding to devices of different sizes were defined.

B) In next step the devices were again exposed, but also rectangles corresponding to bond-pads and thin lines connecting each bond-pad to its corresponding device.

After exposure and development, contacts were deposited using Sputterer - AJA Orion 5. First 3 nm nickel was deposited and on top of that 75 nm ITO. Lift-off with acetone was then used to remove metal deposited in areas not defined in the e-beam resist. After optical inspection the sample was put additional time in acetone and ultra-sonic bath if needed. Then a diamond pen was used to scratch down to the GaN buffer layer in order to enable deposition of an n-contact, which was deposited by sputtering 5 nm Ti and 150 nm Au in an area defined by a shadow mask. In Figure 4.28 the process steps are visualised, but for the case of an etched n-contact (instead of scratching with a diamond pen).

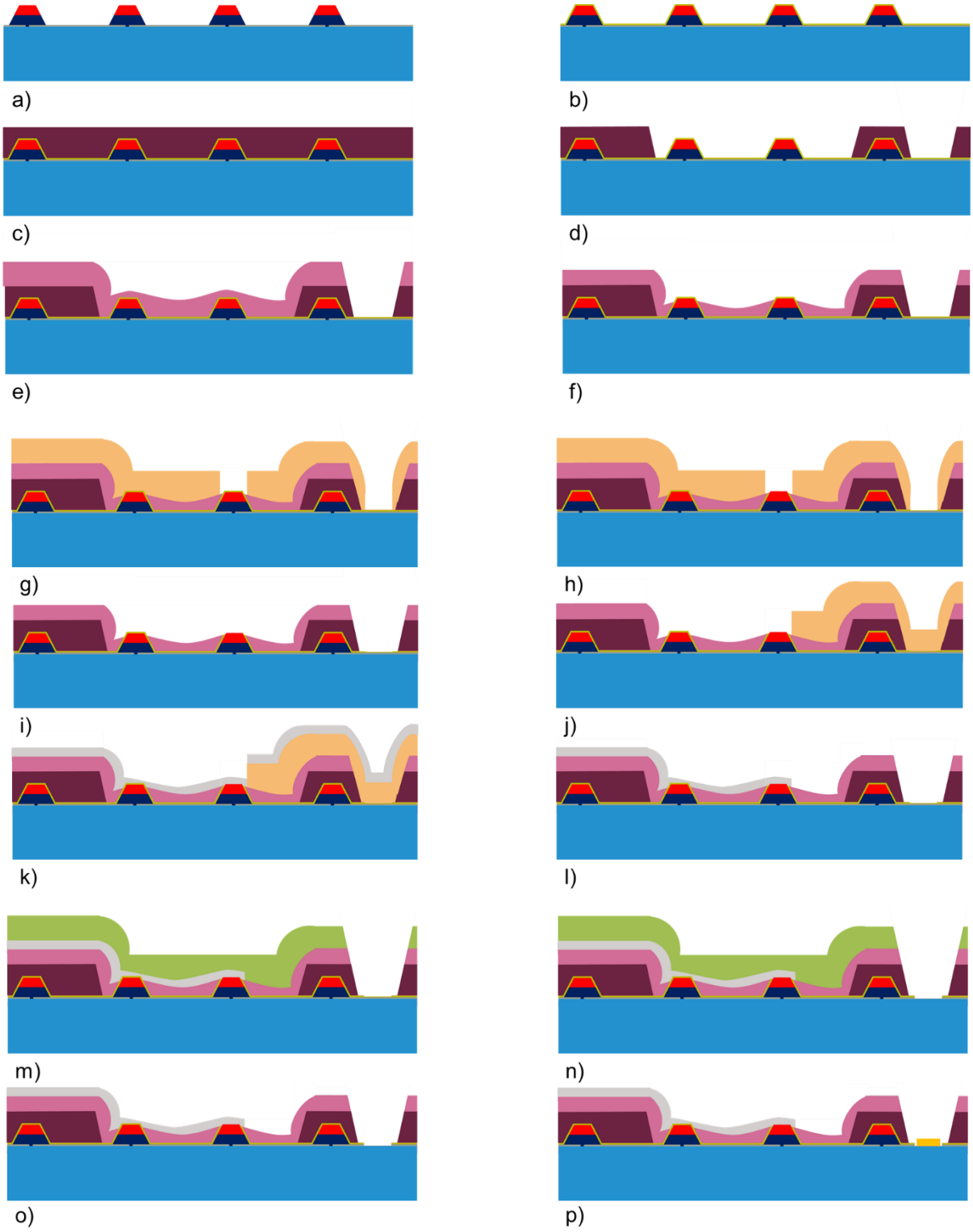
a)
b)
c)
d)
e)
f)
g)
h)
i)
j)
k)
l)
m)
n)
o)
p)

Figure 4.28
Sketches of the different process steps in fabrication of devices of different sizes. The thick light blue layer corresponds to the GaN buffer layer and the thin grey layer corresponds to the Si_3N_4 growth mask. The red and dark blue layers correspond to the p- and n-barriers respectively.

a) *RTP (700 °C, 10 min)*
b) *ALD (400 cycles Al_2O_3)*
c) *Deposition of spacer layer 1 (S1828)*
d) *Definition of openings in spacer layer 1 by UV-lithography. The openings correspond to the device area and the area where the n-contact will be*
e) *Deposition of spacer layer 2 (S1805) and definition of opening for the n-contact*
f) *Etch back of spacer layer 2 using O_2 plasma*
g) *Deposition of e-beam resist (PMMA), and definition of openings for devices and for the n-contact*
h) *BOE etching, which removes the oxide layer on top of platelets within devices as well as in the area defined for the n-contact*
i) *Stripping of e-beam resist (acetone, 1 h)*
j) *Deposition of e-beam resist (PMMA), and definition of areas were the top contact will be.*
k) *Sputtering of top contact (Ni/ITO)*
l) *Lift-off with acetone (1 h)*
m) *Deposition of etch mask (S1813) and definition of opening for n-contact*
n) *Etching of growth mask (RIE CHF_3)*
o) *Stripping of etch mask using Remover 1165*
p) *Sputtering of n-contact (Ti/Au) in an area defined by a shadow mask*

The main drawback with this design is that the thickness of spacer layer 2 (S1805) will vary in the device area defined in spacer layer 1. Due to bunching of the resist, the resist will be thicker in the outer parts of the device area compared to the central part, see Figure 4.29. Most of the devices defined by EBL ended up outside of the area where the resist was sufficiently etched and therefore did not get their oxide layer etched even though the openings in the e-beam resist were properly defined. For subsequent samples this problem was solved by placing the devices closer to the centre of the UV-lithography defined opening in spacer layer 1 (another solution is to change the order of the spacer layers, so that the device area is defined in the second layer instead of in the first). In Figure 4.30 the EBL defined openings in the resist is shown and Figure 4.31 verifies that the alignment during EBL is good. Figure 4.32 shows a finished sample. The UV-lithography defined opening in spacer layer 1 and all devices are shown as well as remaining unwanted metal deposition in the area where alignment was performed during EBL.

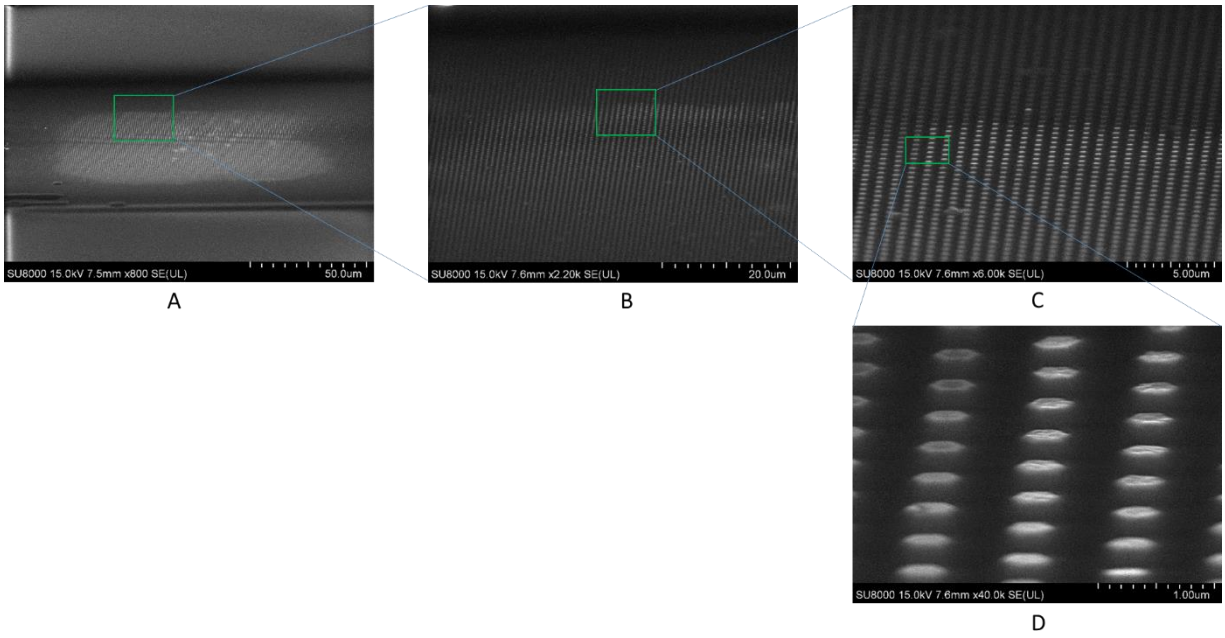

Figure 4.29
SEM images of the sample after BOE and stripping of e-beam resist.

- *A) Image showing the opening in spacer layer 1 (S1828). The bright part in the centre of the opening corresponds to the area where spacer layer 2 (S1805) is sufficiently etched, so that the top of the platelets are free from resist.*
- *B) In this image three different scales of grey are visible, corresponding to platelets covered by spacer layer 2 (darkest grey), platelets which are not covered by spacer layer 2 but were covered by the e-beam resist and therefore have not got their oxide layer etched (brighter grey), and platelets that have got the oxide layer etched (brightest grey).*
- *C) In this image the three different scales of grey are even more visible than in image B.*
- *D) Image showing platelets that have not got the oxide layer etched (left part of the image) and platelets that have got the oxide layer etched (right part of the image).*

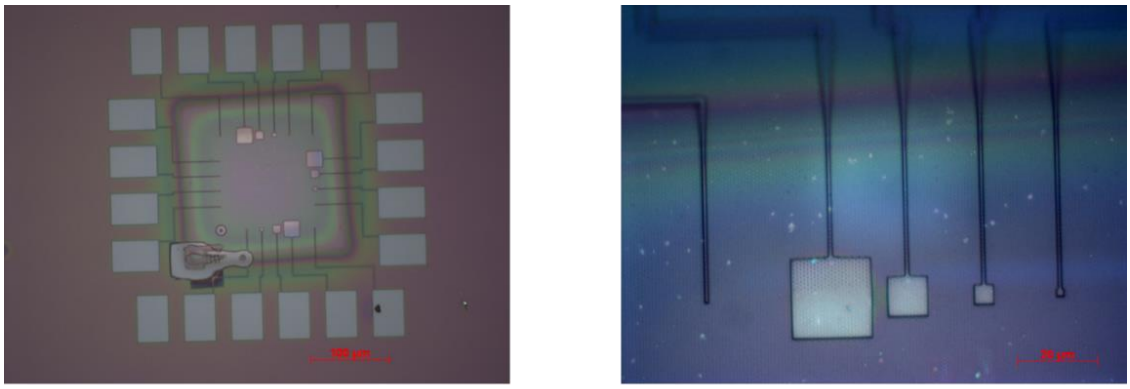

A B

Figure 4.30

Images showing the openings in the e-beam resist after definition of connections, bond pads and devices.

A) The opening in the centre corresponds to the opening in spacer layer 1 (S1828). The other openings correspond to openings defined by EBL. The EBL pattern was aligned according to the platelet array and the opening in spacer layer 1 was aligned according to the edge of the chip (and not with as high precision), which is the reason why the edge of the opening in spacer layer 1 is not aligned with the EBL pattern. The opening in the e-beam resist in the bottom left corner of the opening in spacer layer 1, is due to exposure of the resist during alignment.

B) Image showing the different devices sizes. It is also possible to see that not all platelets in the devices have got their oxide layer etched, which is because the thickness of spacer layer 2 increases in the outer parts of the opening in spacer layer 1. For example the bottom part of the largest device looks brighter than the top part of the device, corresponding to etched and non-etched platelets respectively.

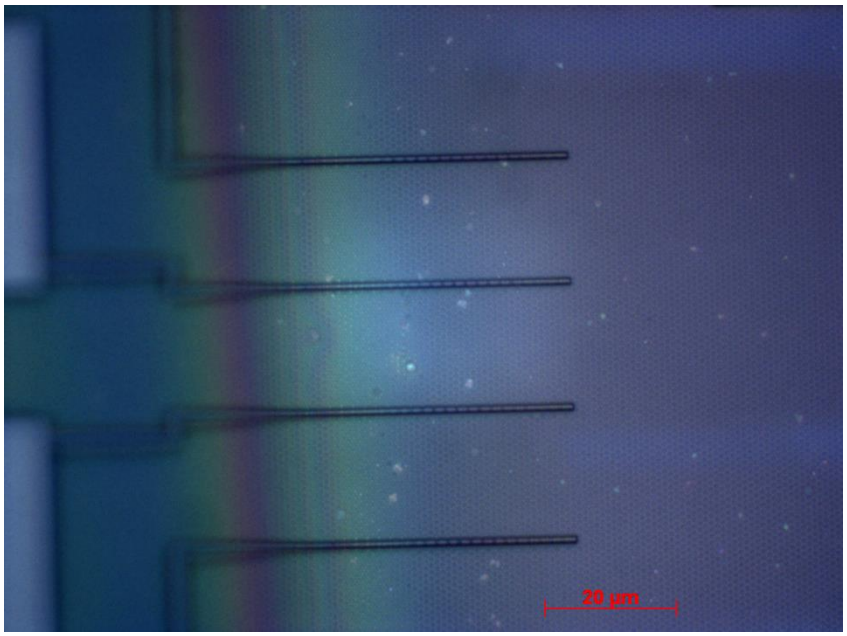

Figure 4.31
Image showing that the alignment looks good. It is possible to see that the opening for the connection follows one row in the platelet array.

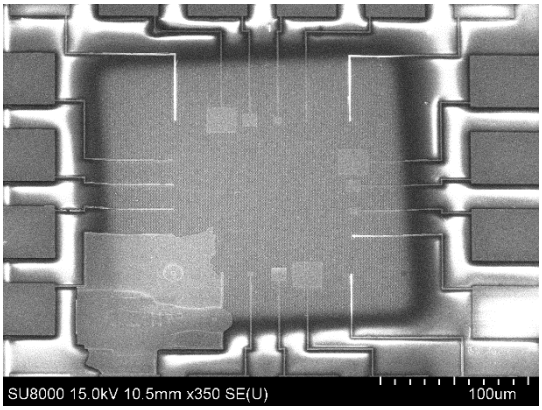

Figure 4.32
SEM image of a finished sample showing the UV-lithography defined opening in spacer layer 1 (S1828). All devices are shown as well as remaining unwanted metal deposition in the bottom left of the image. In this area alignment was performed during EBL which is the reason why metal remains in this area (during alignment this area was exposed, and therefore metal deposited in this area remains after lift-off).

IV-characteristics of all working (conducting) single platelet devices looks very good. The rectification is excellent and the current is in principle zero in the reverse direction, see Figure 4.33 A-B.

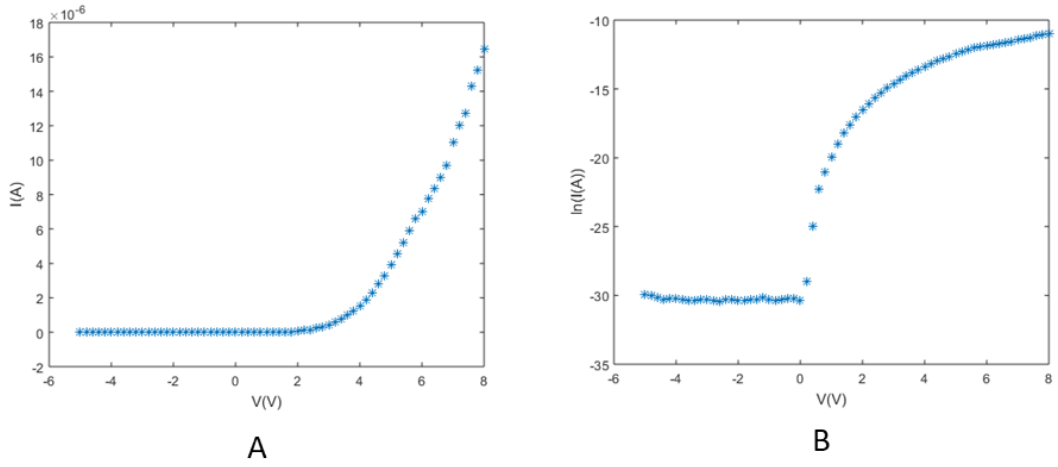

Figure 4.33
IV-curve for one of the single platelet devices. The IV-characteristics of all single platelet devices show either excellent rectification or conduct no current at all.

By comparing Figure 4.33 with Figure 2.3 we can see that the IV-curve of the single platelet devices resembles the case of an ideal diode influenced by series resistance. The high series resistance (200 kΩ, estimated from Figure 4.33 A at 6-8 V) consists of the resistance in the contact to the p-side of the platelets, the resistance in the connection from bond pad to device and the resistance in the contact to the n-side (GaN buffer layer). The length of the connections between the bond pads and devices varies from device to device but is in the interval 80 to 180 µm, which from the calculated resistivity of the top contact (chapter 4.4) gives a series resistance between 9,6 and 22 kΩ and the contact resistance of the n-contact is quite low, around 40-45 ohm, see Figure 4.17 C-D. Most of the series resistance arises therefore in the contact between the top contact and the p-side of the platelets.

Devices consisting of four platelets show either very good rectification or almost none rectification at all (appendix A2). Some of the devices consisting of 25 platelets show good rectification but for others the current is approximately the same in forward and reverse direction (appendix A3). The same behaviour is seen for devices consisting of 100 platelets (appendix A4) and 400 platelets (appendix A5).

In order to investigate if there are any structural differences between rectifying and non-rectifying devices, SEM inspection was performed, see Figure 4.34. From the inspection it was not possible to see any differences and further investigation is needed, maybe cross-section

images of rectifying and non-rectifying devices would clarify the different electrical behaviour of the devices.

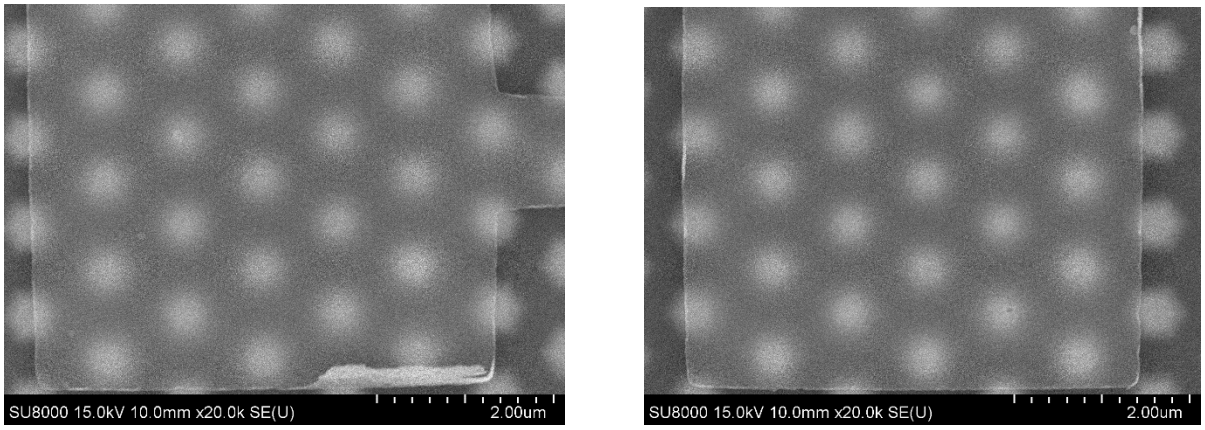

A B

Figure 4.34
SEM-images comparing a non-rectifying device (A) and a rectifying device (B). Both devices consist of 25 platelets and no structural difference between the devices is seen.

The IV-curves look in principle the same regardless if the n-contact consisting of Ni/ITO or Ti/Au is used (appendix A3). Further indicating that the n-contact does not limit the device performance. In some cases the current actually is lower when the better n-contact (Ti/Au) is used (appendix A4, appendix A5). Worth noting is that all measurements using the Ni /ITO n-contact were performed first and then measurements with the Ti/Au n-contact were performed. Therefore one possible explanation for why the current becomes lower when the better n-contact is used, is that the properties of the platelets change during measurements. Another indication of this is that the rectification seems to decrease after a slightly higher voltage (5 V) has been applied in the reverse direction (appendix A1, appendix A3, appendix A4).

The ideality factor (chapter 2) can be extracted from the linear part of the IV-curves plotted in logarithmic scale, and for the rectifying devices the ideality factor varies from 2 to 7. High ideality factors are usually found in III-nitride LEDs which could be due to multiple junctions in the device [23]. For instance there could be additional heterojunctions beyond the quantum well due to different In compositions in the layers or a Schottky barrier at the top contact/p-InGaN junction [23].

5 Conclusion

This chapter gives an overall conclusion of the results, presents a potential improvement of the device design and ends with an outlook.

The main goal of this Master's thesis was to develop and evaluate an LED device design suitable for permanent connections by bonding in order to enable fabrication of a packaged LED demonstrator. The implemented device design works well. Parasitic currents outside the active area are negligible and the devices show much improved stability (bright and stable emission for tens of minutes) compared to previous designs. The thick lifted bond pads outside of the device area enable easy bonding. The device design is therefore suitable for permanent connections by bonding and the goal of this Master's thesis is thus fulfilled.

From data and discussion it is clear that the uniformity is very important for the performance of the device. This type of device puts extremely high demands on the uniformity and homogeneity. Layer thicknesses need to be controlled with nanometre precision over distances in the millimetre scale and hundreds of thousands of separate diodes need to have identical properties. The larger the device area the greater the probability of inhomogeneity, which is the reason why none of the large area devices (400x400 μm^2, 200x200 μm^2), some of the medium sized devices (20x20 μm^2, 10x10 μm^2, 5x5 μm^2, 2x2 μm^2) and all working single platelet devices are rectifying.

A possible improvement of the device design, which maybe could solve the problem with height differences between the platelets and uneven thicknesses of the spacer layers, would be to grow an insulating layer of SiO_2 which covers the platelets and then use CMP to polish down the layer until the p-side of the platelets becomes exposed. Then a spacer layer is deposited and an opening for the device area as well as for the n-contact are defined by UV-lithography. The top contact is then deposited followed by deposition of an etch mask and etching to the GaN buffer layer. The etch mask is then stripped and bond pads are deposited in areas defined by shadow masks, see Figure 5.1. A possible drawback of this design is the risk of leakage to platelets outside of the device area, which will depend on the conductivity of the spacer layer and its thickness. Another drawback is absorption of light by the insulating layer (SiO_2). Further work is also necessary to optimise the homogeneity of the thicknesses of the barrier layers, quantum wells and doping levels.

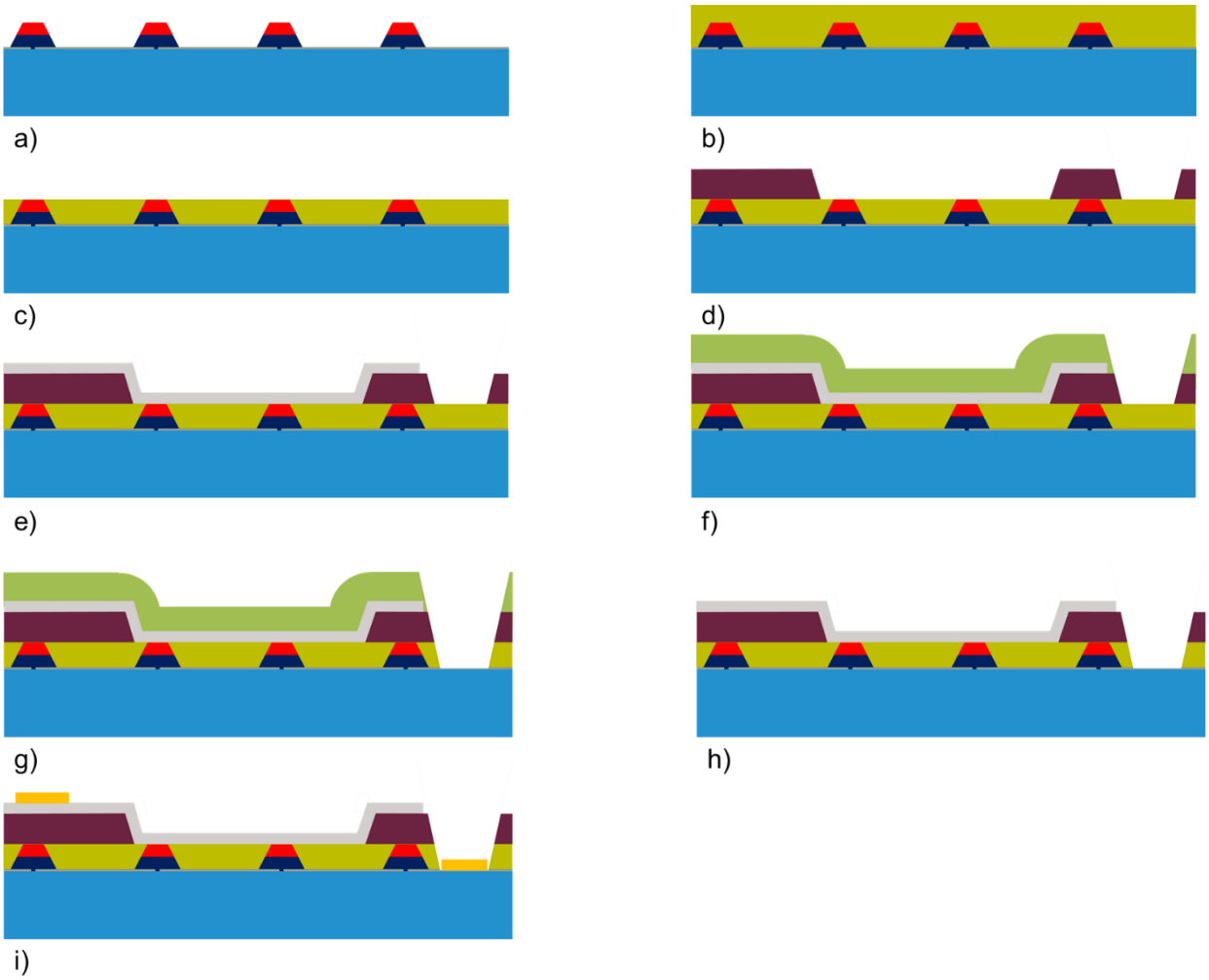

Figure 5.1
Sketches of the different process steps in fabrication of a potential improved device design. The thick light blue layer corresponds to the GaN buffer layer and the thin grey layer corresponds to the Si_3N_4 growth mask. The red and dark blue layers correspond to the p- and n-barriers respectively.

- *a) RTP (700 °C, 10 min)*
- *b) Growth of insulating layer (LPCVD, SiO_2)*
- *c) Chemical mechanical polishing (CMP) until the p-side of the platelets becomes exposed*
- *d) Deposition of a spacer layer (S1828) and definition of openings for the device area as well as for the n-contact*
- *e) Deposition of top contact (Ni/ITO) in an area defined by sputtering through a shadow mask*
- *f) Deposition of etch mask (S1813) and definition of opening for n-contact*
- *g) Etching of insulating layer and growth mask (RIE, CHF_3)*
- *h) Stripping of etch mask using Remover 1165 followed by ultra-sonic bath*
- *i) Deposition of bond pads (Ti/Au) in areas defined by a shadow mask*

The light extraction efficiency is a very important property of an LED. Nanostructured surfaces are known to improve light extraction [17]. The light extraction from platelet structures would be an interesting topic to explore in order to optimise the LED structure further. In this project devices were fabricated either on sapphire substrates or on silicon substrates. The results from the electro-optical characterisation are similar regardless which substrate that are used, but the light output from devices fabricated on sapphire substrates looks much brighter than the light output from devices fabricated on silicon substrates, compare Figure 4.16 A (sapphire) and Figure 4.16 B (silicon). The reason to the brighter light output is probably due to absorption of more light in the silicon substrate compared to the absorbed light in the sapphire substrate.

Another interesting phenomenon is that the properties of the platelets seem to change during measurements, especially if a slightly higher voltage is applied in the reverse direction. It is hard to say what really happens but it is clear that the device performance becomes worse.

The final question is then, what potential has LEDs based on InGaN and GaN platelets? The greatest challenge is to grow tens of thousands of platelets of high uniformity and if this is solved these platelets has potential to be used in high efficiency RGB LEDs in the future. While work lies ahead in improving homogeneity, efficiency and device design, this technology is unique in achieving high quality material with very high In content and an extremely small light emission area. Not only are these structures interesting for high-efficiency RGB illumination, but also for microLED displays - potentially with pixel size an order of magnitude smaller than what is possible today. As mentioned in chapter 2.2 there are many advantages of nanowire LEDs compared to conventional planar LEDs, for instance reduced efficiency-droop, reduced piezoelectric polarisation field and together with the light extraction enhancement related to nanostructures this approach has potential to be used in high efficiency lightning. Maybe the end application will not be as RGB LEDs but we believe that this concept has the potential to become an important technology for future high-performance nitride optoelectronics.

6 References

[1] Huang, Min & Yang, Liyu. (2013). **Heat Generation by the Phosphor Layer of High-Power White LED Emitters**. IEEE Photonics Technology Letters. 25. 1317-1320. 10.1109/LPT.2013.2263375.

[2] Jianxun Liu, Hongwei Liang, Xiaochuan Xia, Qasim Abbas, Yang Liu, Yingmin Luo, Yuantao Zhang, Long Yan, Xu Han, Guotong Du.
Anomalous indium incorporation and optical properties of high indium content InGaN grown by MOCVD.
Journal of Alloys and Compounds. Volume 735, 25 February 2018, Pages 1239-1244

[3] Auf der Maur, Matthias & Pecchia, Alessandro & Penazzi, Gabriele & Rodrigues, Walter & Di Carlo, Aldo. (2015). **Unraveling the "Green Gap" problem: The role of random alloy fluctuations in InGaN/GaN light emitting diodes**.
Physical Review Letters. 116. 10.1103/PhysRevLett.116.027401.

[4] Jurga Juodkazytė, Benjaminas Šebeka, Irena Savickaja, Arūnas Kadys, Edgaras Jelmakas, Tomas Grinys, Saulius Juodkazis, Kęstutis Juodkazis, Tadas Malinauskas.
$In_xGa_{1-x}N$ performance as a band-gap-tunable photo-electrode in acidic and basic solutions.
Solar Energy Materials and Solar Cells. Volume 130, November 2014, Pages 36-41

[5] Schubert, E. F. **Light-Emitting Diodes**. Cambridge University Press (2006)

[6] Hultin, O. (2018). **Nanostructures for Optoelectronics: Device Fabrication and Characterization.** Division of Solid State Physics, Department of Physics, Lund University, Box 118, SE-221 00 Lund, Sweden

[7] Z. Bi, A. Gustafsson, F. Lenrick, D. Lindgren, O. Hultin, L.R. Wallenberg, B.J. Ohlsson, B. Monemar, L. Samuelson. **High In-content InGaN nano-pyramids: Tuning crystal homogeneity by optimized nucleation of GaN seeds.**
Journal of Applied Physics 123, 025102 (2018).

[8] Zhaoxia Bi, Filip Lenrick, Jovana Colvin, Anders Gustafsson, Olof Hultin, Ali Nowzari, Taiping Lu, Reine Wallenberg, Rainer Timm, Anders Mikkelsen, B. Jonas Ohlsson, Kristian Storm, Bo Monemar, and Lars Samuelson. **InGaN Platelets: Synthesis and Applications toward Green and Red Light-Emitting Diodes**
Nano Letters 2019 19 (5), 2832-2839
DOI: 10.1021/acs.nanolett.8b04781

[9]Bahaa E.A. Saleh, Malvin Carl Teich. **Fundamentals of photonics**. Wiley Interscience (2007)

[10] Monemar, B., Ohlsson, B. ., Gardner, N. . & Samuelson, L. in Semiconductors and Semimetals : Semiconductor Nanowires II: Properties and Applications 227–271 (Academic Press/Elsevier, 2016).

[11] J. Ryou et al., "**Control of Quantum-Confined Stark Effect in InGaN-Based Quantum Wells**," in IEEE Journal of Selected Topics in Quantum Electronics, vol. 15, no. 4, pp. 1080-1091, July-aug. 2009.
doi: 10.1109/JSTQE.2009.2014170

[12] B. Monemar, B.E. Sernelius, **Defect related issues in the "current roll-off" in InGaN based light emitting diodes**
Appl. Phys. Lett., 91 (2007), p. 181103

[13] Robert Koester, Jun-Seok Hwang, Damien Salomon, Xiaojun Chen, Catherine Bougerol, Jean-Paul Barnes, Daniel Le Si Dang, Lorenzo Rigutti, Andres de Luna Bugallo, Gwénolé Jacopin, Maria Tchernycheva, Christophe Durand, and Joël Eymery, **M-Plane Core–Shell InGaN/GaN Multiple-Quantum-Wells on GaN Wires for Electroluminescent Devices**
Nano Letters 2011 11 (11), 4839-4845
DOI: 10.1021/nl202686n

[14] Renjie Wang, Hieu P. T. Nguyen, Ashfiqua T. Connie, J. Lee, Ishiang Shih, and Zetian Mi, "**Color-tunable, phosphor-free InGaN nanowire light-emitting diode arrays monolithically integrated on silicon,**" Opt. Express 22, A1768-A1775 (2014)

[15] Templier, F. (2016) **GaN-based emissive microdisplays: A very promising technology for compact, ultra-high brightness display systems**. *Jnl Soc Info Display*, 24: 669– 675. doi: 10.1002/jsid.516

[16] S. Zhao, R. Wang, S. Chu and Z. Mi, "**Molecular Beam Epitaxy of III-Nitride Nanowires: Emerging Applications From Deep-Ultraviolet Light Emitters and Micro-LEDs to Artificial Photosynthesis,**" in IEEE Nanotechnology Magazine, vol. 13, no. 2, pp. 6-16, April 2019.
doi: 10.1109/MNANO.2019.2891370

[17] Seung Hwan Kim, Hyun Ho Park, Young Ho Song, Hyung Jo Park, Jae Beom Kim, Seong Ran Jeon, Hyun Jeong, Mun Seok Jeong, and Gye Mo Yang, "**An improvement of light extraction efficiency for GaN-based light emitting diodes by selective etched nanorods in periodic microholes**," Opt. Express 21, 7125-7130 (2013)

[18] Zhao Chao, Ng Tien Khee, Prabaswara Aditya, Conroy Michele, Jahangir Shafat, Frost Thomas, O'Connell John, Holmes Justin D, Parbrook Peter J, Bhattacharya Pallab, Ooi Boon S. **An enhanced surface passivation effect in InGaN/GaN disk-in-nanowire light emitting diodes for mitigating Shockley–Read–Hall recombination,** Nanoscale, vol. 7, issue 40, pp. 16658-16665, 2015
doi: 10.1039/C5NR03448E

[19] Hieu Pham Trung Nguyen, Mehrdad Djavid and Zetian Mi. **Nonradiative Recombination Mechanism in Phosphor-Free GaN-Based Nanowire White Light Emitting Diodes and the effect of Ammonium Sulfide Surface Passivation.**
doi: 10.1149/05302.0093ecst
ECS Trans. 2013 volume 53, issue 2, 93-100

[20] Chris G Van de Walle, Catherine Stampfl, Jörg Neugebauer. **Theory of doping and defects in III–V nitrides.** Journal of Crystal Growth, Volumes 189–190, 15 June 1998, Pages 505-510

[21] Sze, S. and Lee, M. (2013). **Semiconductor devices: Physics and Technology**. 3rd ed. Singapore: John Wiley & Sons.

[22] Ahmad Hadi Ali; Zainuriah Hassan; Ahmad Shuhaimi. (2018). **Enhancement of optical transmittance and electrical resistivity of post-annealed ITO thin films RF sputtered on Si.** Applied Surface Science, ISSN: 0169-4332, Vol: 443, Page: 544-547.

[23] Jay M. Shah, Y.-L. Li, Th. Gessmann, and E. F. Schubert. **Experimental analysis and theoretical model for anomalously high ideality factors (n≫2.0) in AlGaN/GaN p-n junction diodes.**
Journal of Applied Physics 94, 2627 (2003)

7 Appendices

Appendix A1 Single platelet devices

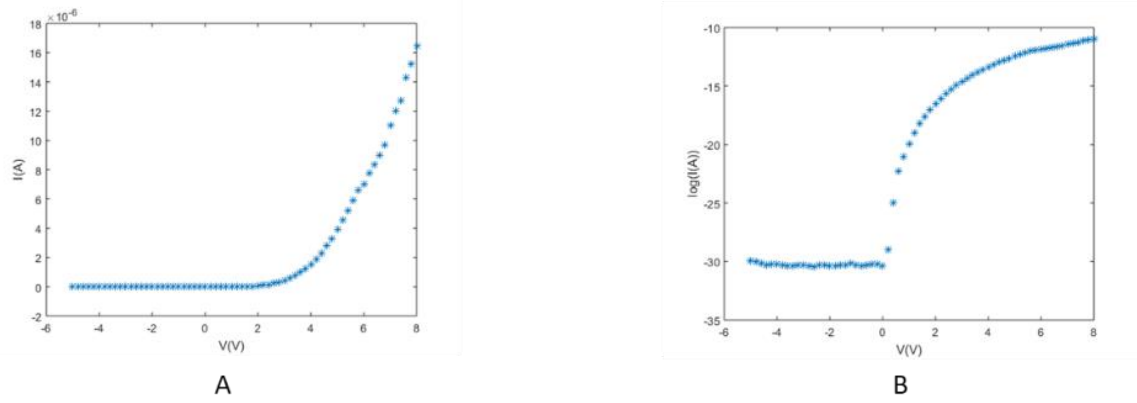

Figure 1
IV-curve for one of the single platelet devices. The IV-characteristics for all single platelet devices show either excellent rectification or conduct no current at all.

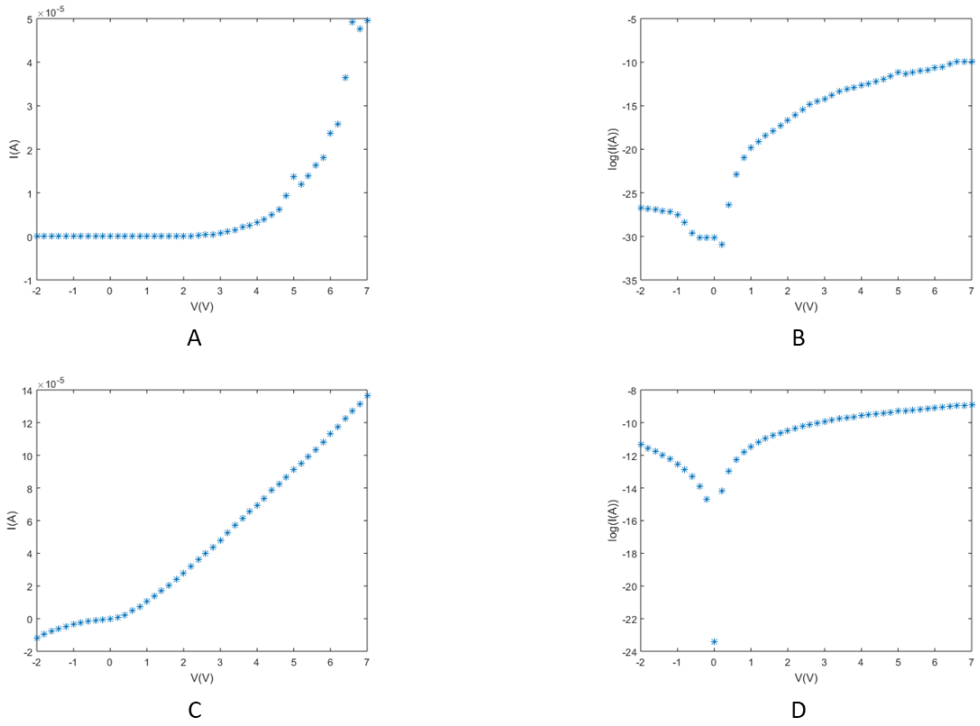

Figure 2
IV-characteristics for a single platelet device before (A-B) and after (C-D) 5 V has been applied in the reverse direction. The rectification is much better before 5 V has been applied in the reverse direction.

Appendix A2 Devices consisting of four platelets

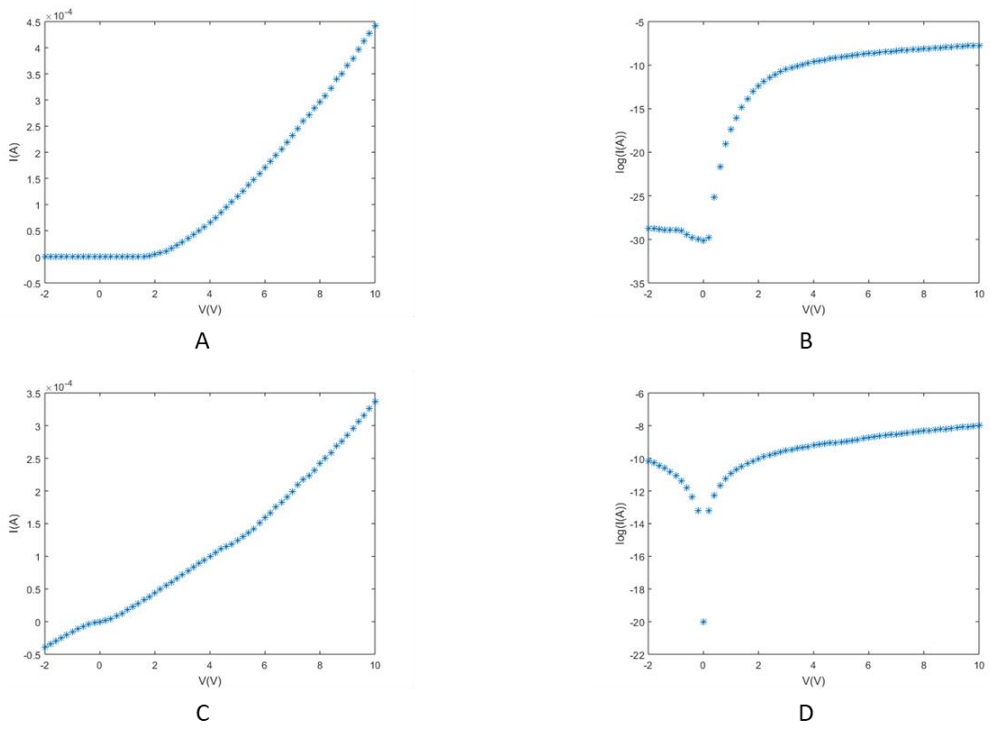

Figure 1

IV-characteristics for two devices consisting of four platelets each. One of the devices (A-B) shows very good rectification while the other device (C-D) almost shows no rectification at all.

Appendix A3 Devices consisting of 25 platelets

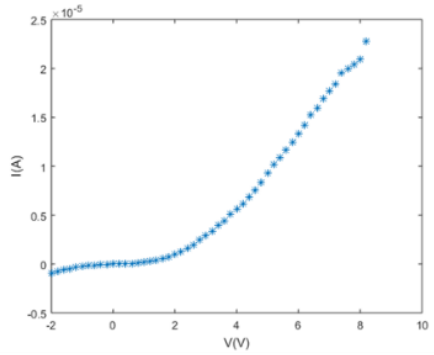

A

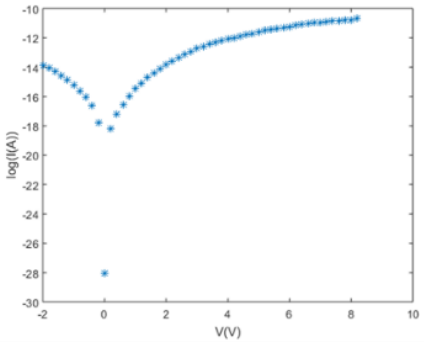

B

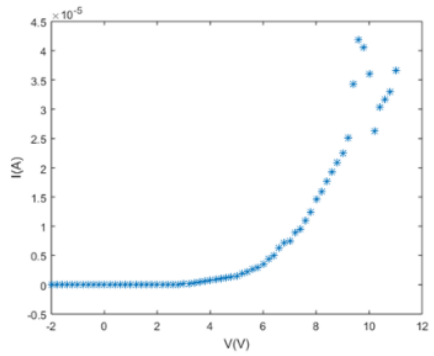

C

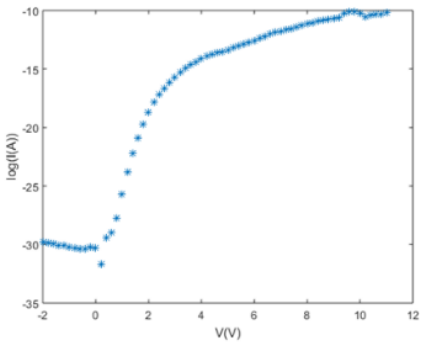

D

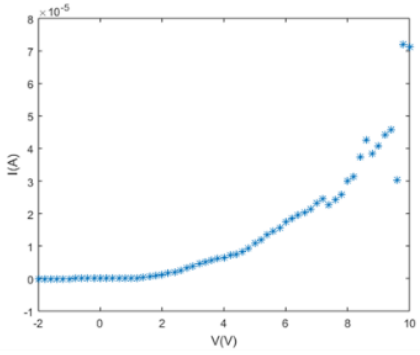

E

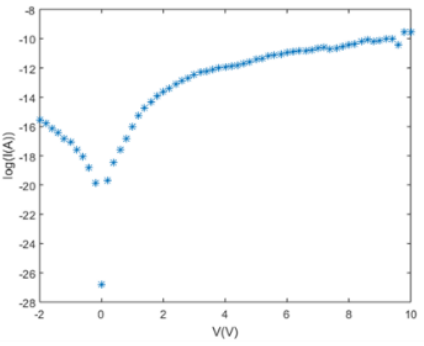

F

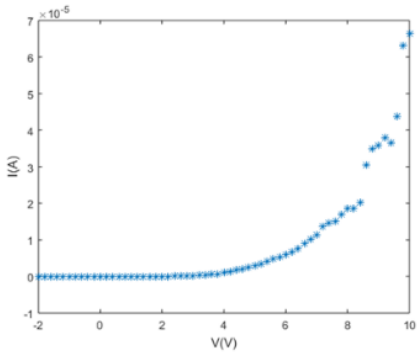

G

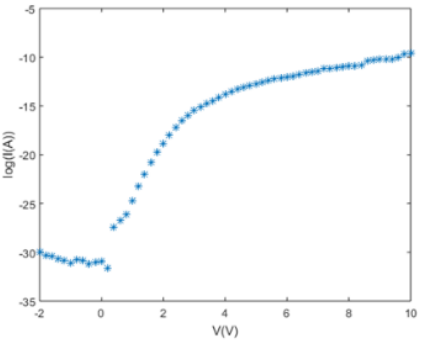

H

Figure 1

IV-characteristics for two different devices consisting of 25 platelets. Figure A-B and E-F correspond to one device, C-D and G-H correspond to the other device. For A-B and C-D an n-contact consisting of Ni and ITO was used, and for E-F and G-H an n-contact consisting of Ti and Au was used.

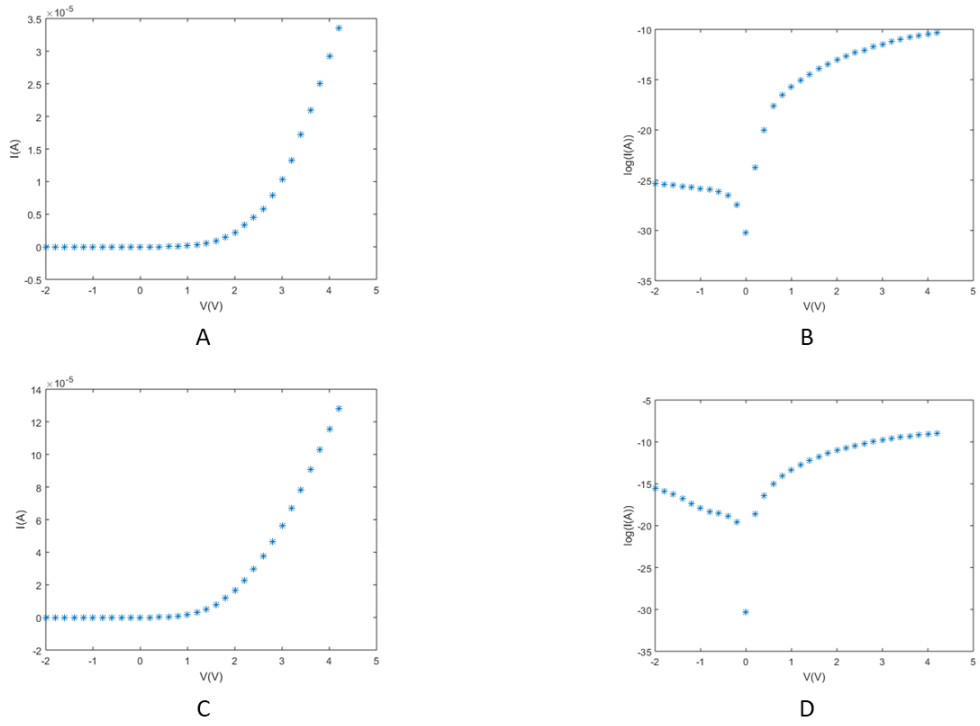

Figure 2

IV-characteristics for a device, consisting of 25 platelets, before (A-B) and after (C-D) 5 V has been applied in the reverse direction. The rectification is much better before 5 V has been applied in the reverse direction.

Appendix A4 Devices consisting of 100 platelets

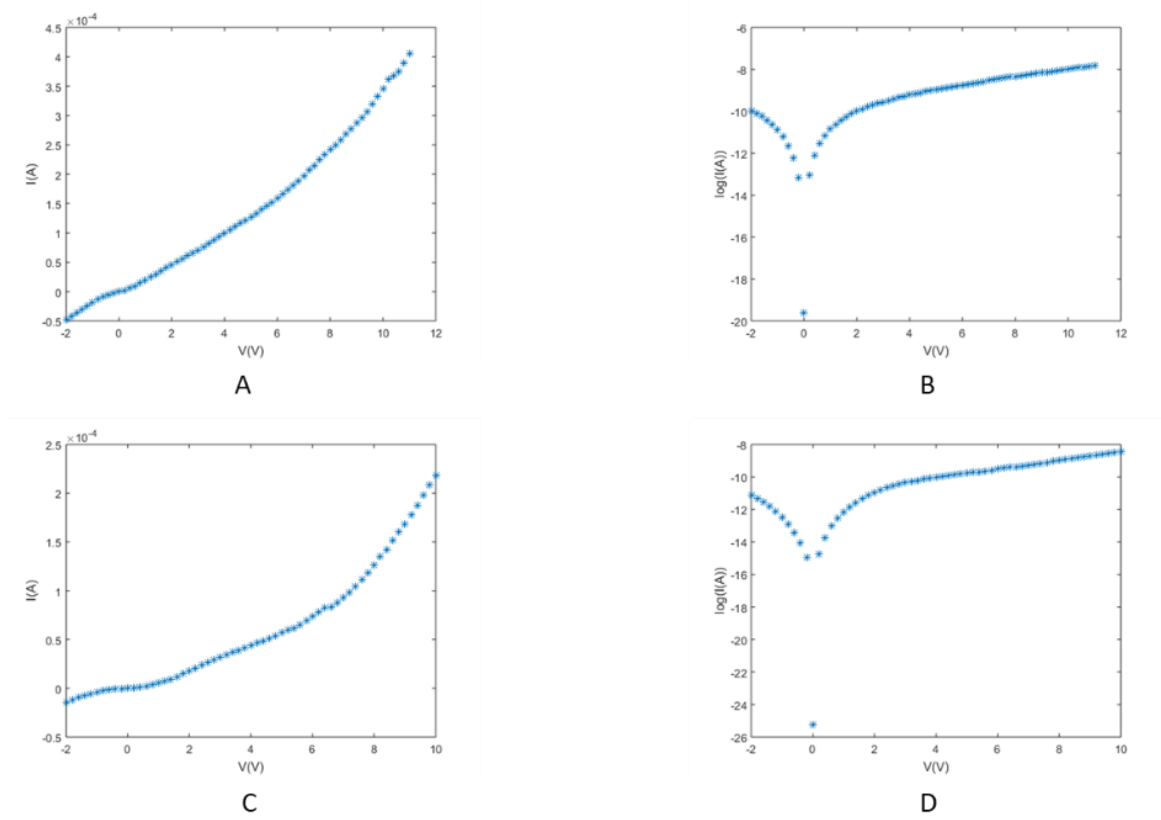

Figure 1
IV-characteristics for one of the devices consisting of 100 platelets. For A-B an n-contact consisting of Ni and ITO was used and for C-D an n-contact consisting of Ti and Au was used.

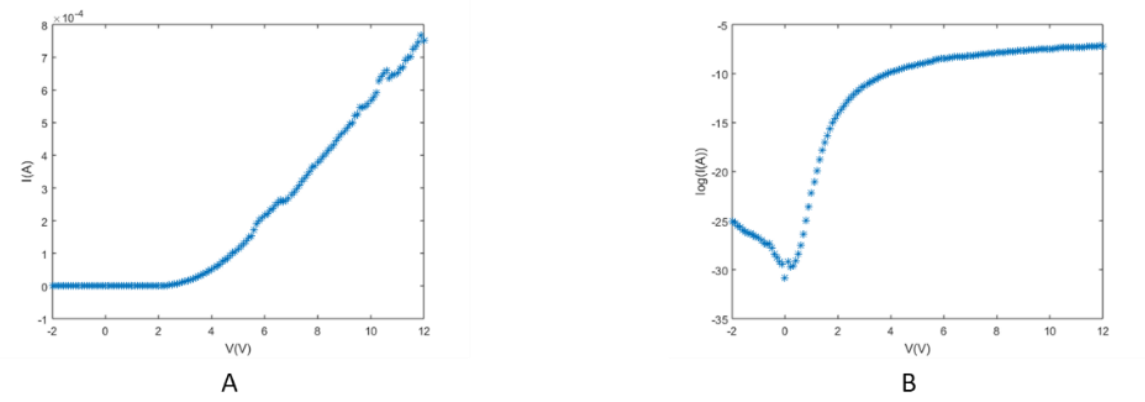

Figure 2
IV-characteristics for one of the devices consisting of 100 platelets (n-contact consisting of Ti/Au was used).

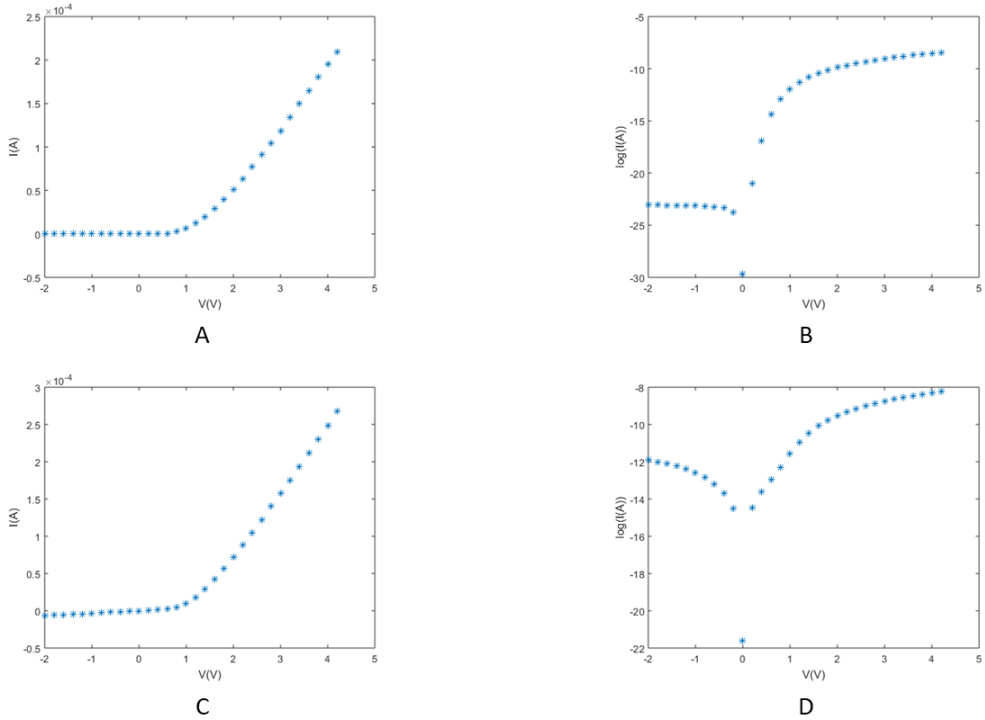

Figure 3

IV-characteristics for a device consisting of 100 platelets, before (A-B) and after (C-D) 5 V has been applied in the reverse direction. The rectification is much better before 5 V has been applied in the reverse direction.

Appendix A5 Devices consisting of 400 platelets

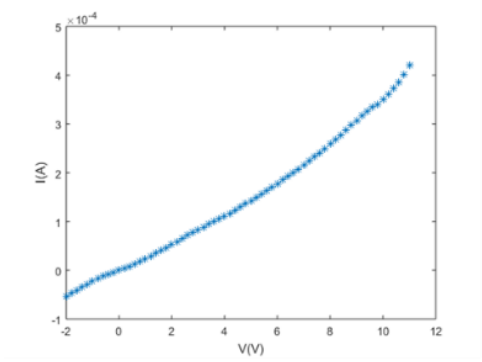

A

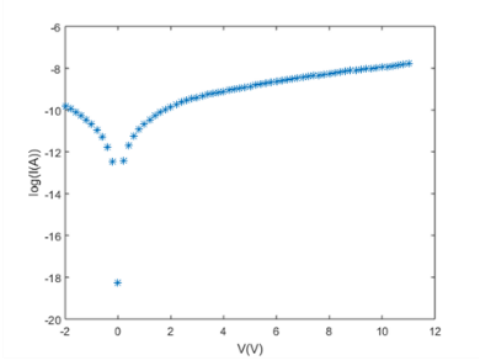

B

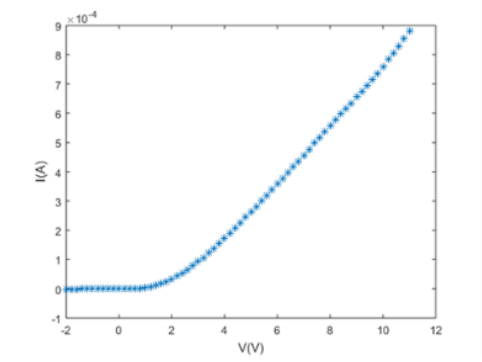

C

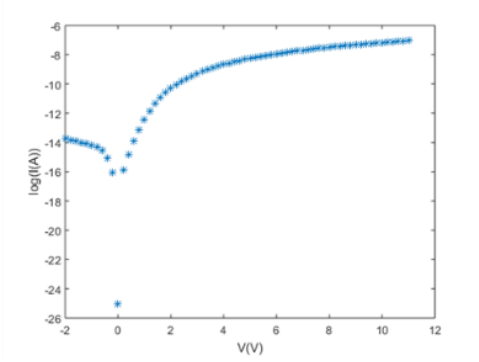

D

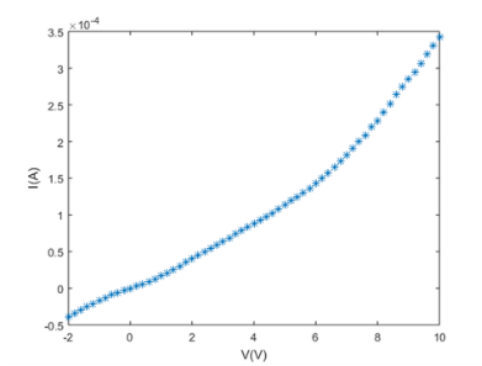

E

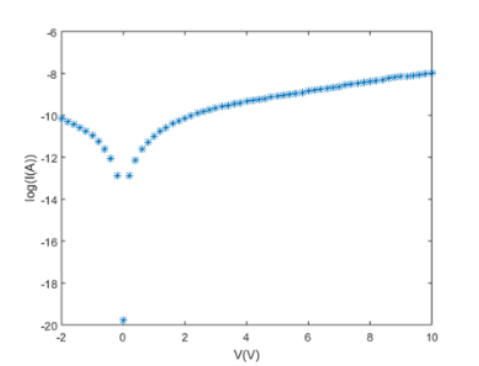

F

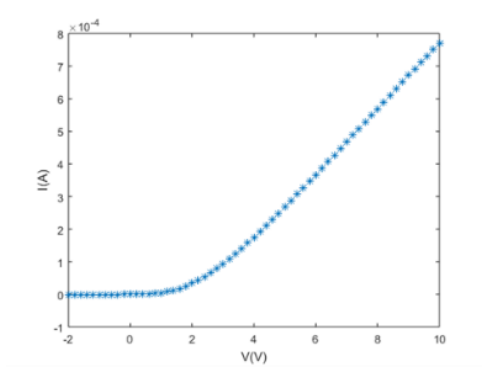

G

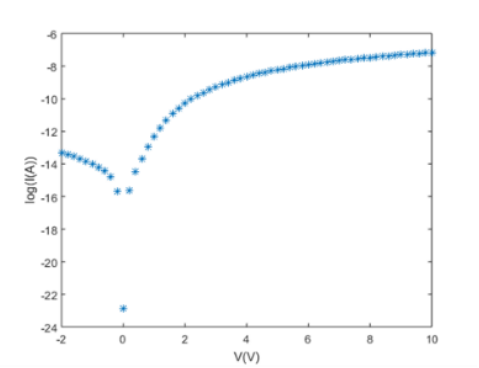

H

Figure 1

IV-characteristics for two different devices consisting of 400 platelets. Figure A-B and E-F correspond to one device, C-D and G-H correspond to the other device. For A-B and C-D an n-contact consisting of Ni and ITO was used, and for E-F and G-H an n-contact consisting of Ti and Au was used.

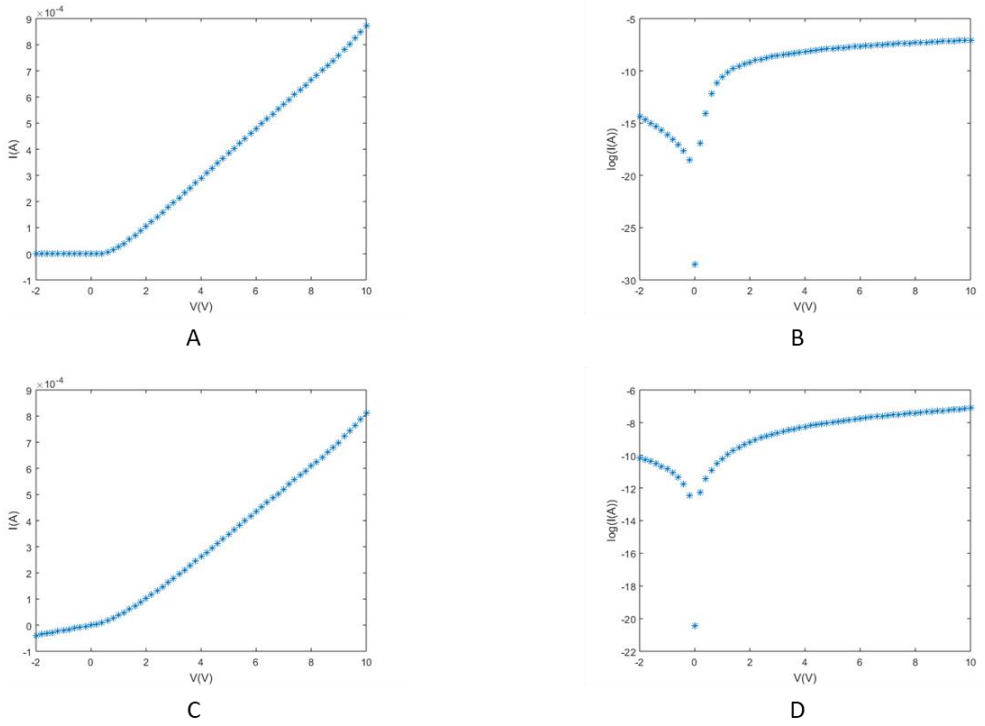

Figure 2

IV-characteristics for two devices consisting of 400 platelets each. One of the devices (A-B) shows very good rectification while the other device (C-D) shows almost no rectification at all.